Mineralogy and Petrology (2020) 114:15–38
https://doi.org/10.1007/s00710-019-00688-6

ORIGINAL PAPER

Mineral chemistry, petrogenesis and evolution of the Ghorveh-Seranjic skarn, Northern Sanandaj Sirjan Zone, Iran

Zohreh Alaminia[1] · Behzad Mehrabi[1] · Seyed Mohammad Hossein Razavi[1] · Francesca Tecce[2]

Received: 31 December 2017 / Accepted: 20 September 2019 / Published online: 14 December 2019

Abstract

The Ghorveh-Seranjic (GS) skarn is located in the northern part of the Sanandaj-Sirjan zone, NW Iran, which is part of Alpine-Himalaya orogenic belt. The GS metamorphic complex is the oldest unit in the GS area composed of marble, dolomitic marble, greenschist, and amphibolite of Early Jurassic age. The complex is intruded by NW-SE trending Late Jurassic peraluminous granitoids, which caused contact metamorphism and resulted in the development of skarn, hornfels and crystallization of marble. The skarn is showing distinct textural, mineralogical and geochemical zonation. At least four stages of skarn development have been recognized; stage I, clinopyroxene+garnet±vesuvianite±quartz±calcite±scheelite± pyrrhotite; stage II, garnet+ clinopyroxene +vesuvianite+scheelite±apatite+calcite±pyrrhotite; stage III, amphibole+vesuvianite+epidote+chlorite±quartz ±calcite±pyrrhotite±pyrite±chalcopyrite and stage IV, quartz+calcite±amphibole±epidote±chlorite±pyrite±chalcopyrite. Scheelite occurs in stages 1 and 2 together with garnet and clinopyroxene, and its abundance slightly increases with vesuvianite growth. In general, mineral chemistry of the GS skarn shows enrichment in Ca, Al and Mg. Two types of garnet, clinopyroxene and vesuvianite are identified in the prograde stage within the GS skarn. Variable Mg:Mn:Fe proportions in clinopyroxene of the early prograde stage suggest formation from a relatively homogeneous F-rich volatile phase. Mineralogical documentation of the GS skarn indicates that presence of the F-rich volatile phase affected zoning patterns and mineral abundances. Addition of fluorine increases the solubility of Al in the hydrothermal fluid by forming strong Al-F complexes, causing an increase in vesuvianite instead of clinopyroxene during the late prograde substage, resulting in high garnet/clinopyroxene ratios. The presence of granditic (grossular-andradite) and subcalcic (grossular-almandine-spessartine) garnet during the skarn evolution suggests variable Fe/Mn and Fe^{2+}/Fe^{3+} ratios during the prograde stage of the skarn formation. Subcalcic garnet formed in a relatively reduced environment compared to the granditic garnet. Paragenetic reconstructions indicate that clinopyroxene, garnet and scheelite grew together during the prograde stage. These minerals were stable and coexisted at temperatures between 580 °C and 400 °C and at a $\log fO_2 = -18$ to -28.

Keywords Sanandaj-Sirjan zone · Ghorveh Seranjic · Mineral chemistry · Petrogenesis · Skarn

Introduction

Skarns are calc-silicate rocks that can form during regional or contact metamorphism and from a variety of metasomatic processes involving fluids of magmatic, metamorphic, meteoric, and/or seawater origin (Meinert et al. 2005). Skarn-forming minerals show ranges of compositional variation, reveal important information about skarn-forming environments such as compositions of the protolith and associated igneous rocks, depth of formation, oxygen fugacity and type of skarn (Zuo et al. 2015; Kamvong and Zaw 2009; Lehrmann et al. 2009; Grammatikopoulos and Clark 2006; Meinert et al. 2005; Ciobanu and Cook 2004; Cepedal et al. 2000; Meinert, 1995; Einaudi and Burt 1982; Shimazaki 1980). Skarn-forming minerals may provide a continuous record of the physicochemical evolution of a skarn system. Details of skarn mineralogy and zonation can be used to construct deposit-specific exploration models.

Editorial handling: C. Hauzenberger

✉ Zohreh Alaminia
zoalaminia@gmail.com; z.alaminia@yahoo.com

[1] Department of Geochemistry, Faculty of Earth Sciences, Kharazmi University, 43, Shahid Mofatteh Av., Tehran, Iran

[2] Istituto di Geologia Ambientale e Geoingegneria, Consiglio Nazionale delle Ricerche, Piazzale Aldo Moro 5, 00185 Rome, Italy

In the NW-SE trending Sanandaj-Sirjan zone (SSZ), NW Iran, a variety of granitoid bodies emplaced in several stages during Mesozoic times (Mohajjel et al. 2003). Intrusive bodies are widespread and have substantial contact aureoles, which are frequently associated with ore mineralizations including the iron skarn deposit at Zafar-Abad (Barati and Gholipoor 2014), Galali (Barati 2012), Baba-Ali and Hamekasi (Zamanian and Radmard 2016; Payder 2016; Payder et al. 2010; Zamanian. 2007), the Shams-Abad iron deposit (Ghorbani 2013), the Deh–Hossein and Nezam-Abad tungsten-tin (±Cu) deposits (Abdi 2007), the Malayer-Esfahan Pb-Zn district (Ghorbani, 2007; Momenzadeh, 1976) and the Ebrahim-Attar tungsten skarn mineralization (Salami et al. 2013; Daneshvar 2012). The GS Pluton is a major granitoid in the northern part of the SSZ (Fig. 1a), that emplaced at ca. 145.7 ± 1.1 Ma (Azizi et al. 2016) and is associated with an insignificant scheelite occurrence. Although the presence of scheelite mineralization is reported based on regional geochemical sampling (Salami et al. 2013; Daneshvar 2012), there has been no detailed mineralogic, petrographic and geochemical work on the skarn evolution and its mineral chemistry. In this work, we combine a comprehensive dataset based on regional and local geological documentation, petrographic and mineralogical data to relate the genesis of the calc-silicate minerals with the magmatic evolution of the host intrusive body.

Geological setting

The NW-SE trending Sanandaj Sirjan zone (SSZ) is a complex plutonometamorphic structural zone in Iran with 50–100 km width and more than 800 km length. The Main Zagros fault is situated in the southwest of the SSZ and is considered as the suture zone between the Arabian and Iranian plates (Stocklin 1968; Falcon 1974). The SSZ is parallel to the Zagros fold-thrust belt system and extends into Turkey, where it is known as Taurus orogenic belt (Bozkurt et al. 2000; Robertson et al. 2007; Dilek et al. 2010). Basement of the SSZ mainly consists of a Precambrian metamorphic complex, which occurs as a tectonic window (Lake Urumieh: Hassanzadeh et al. 2008, Azizi et al. 2011a; east and north of Golpaygan: Mohajjel and Fergusson 2014) (Fig. 1a). The Jurassic metamorphic rocks are overlain by non-metamorphic Cretaceous rocks, especially in the northwestern part, between Ghorveh and Sanandaj towns (Shakerardakani et al. 2015). From north to south, the SSZ can be divided into two main parts (Fig. 1a): (i) the southern part, consisting of Early to Middle Jurassic deformed metamorphic rocks; and (ii) the northern part composed of various granitoid bodies, which are younger than Early Jurassic (Azizi et al. 2016; Azizi et al. 2015a,b; Shahbazi et al. 2015; Yajam et al. 2015; Azizi and Asahara, 2013; Azizi et al. 2011a,b; Shahbazi et al. 2010; Mahmoudi et al. 2011; Hassanzadeh et al. 2008).

The study area is located in the northern SSZ, in which the main units are marble, dolomitic marble, greenschist, and amphibolite of Early to Middle Jurassic metamorphic age (Mohajjel et al. 2003), which have been invaded by granitoid intrusion (Middle to Late Jurassic) (Fig. 1b). The metamorphic sequence comprises of layers of dark gray metamorphic limestone (0.1 to 5 m) containing organic material and black metachert followed by a massive, kilometer-thick cream-colored metamorphic limestone unit (Figs. 1b). The regional metamorphic complex rocks of Early Jurassic are cut by Middle to Late Jurassic intrusive bodies causing contact metamorphism. The mineral assemblages of regional metamorphism consist of calcite± clinopyroxene± tremolite± epidote ± albite± opaque± titanite showing predominantly greenschist and locally amphibolite facies. Contact metamorphism with mineral assemblages of andalusite+cordierite+biotite+muscovite+K-feldspar+plagioclase occurred at low pressure (< 2 kbar) and at a temperature of 580 ± 50 °C (Sheikhi et al. 2012) evolving hornfels and skarn.

In the study area the regional metamorphic complex is invaded by the GS intrusion resulting in the development of skarn, hornfels and marble. The hornfels zone is limited and only observed in the southwestern part of the study area, as a cordierite bearing hornfels. The Upper Jurassic GS pluton has a sigmoid-shape, NW-SE extending trend, with granite to quartz-monzogranite composition. It contains fine- to medium-grained, rounded/elliptical shaped mafic microgranular enclaves with monzodiorite to monzogabbro composition (Fig. 2a). The pluton is often cut by leucogranite aplite-pegmatite dikes (Fig. 2b) and quartz veins, which have a radial relationship with the contacts (Fig. 2c). The aplite dikes are crosscutting the whole sequence including the skarn zones.

The GS pluton is a peraluminous to strongly peraluminous granitic garnet free intrusion with calc-alkaline to alkaline affinity (Azizi et al. 2016) showing a high degree of fractionation and a high Rb/Sr ratio (average ~21).

At the contact of the GS pluton with marble, a skarn zone of 100 m length and 0.3 to 4 m width is developed. The GS skarn is in direct contact with the pluton, and only in the southeastern part of the district a zone of endoskarn is developed within the pluton (Fig. 2d).

Sampling and analytical methods

A total of 271 samples was collected along traverse lines consecutively from the intrusive bodies towards the wall rocks, to undertake petrographic and mineral chemistry studies. The petrographic studies include identification of mineral assemblages, textures, alteration and metasomatic replacements. Mineral abundance was calculated based on modal mineral

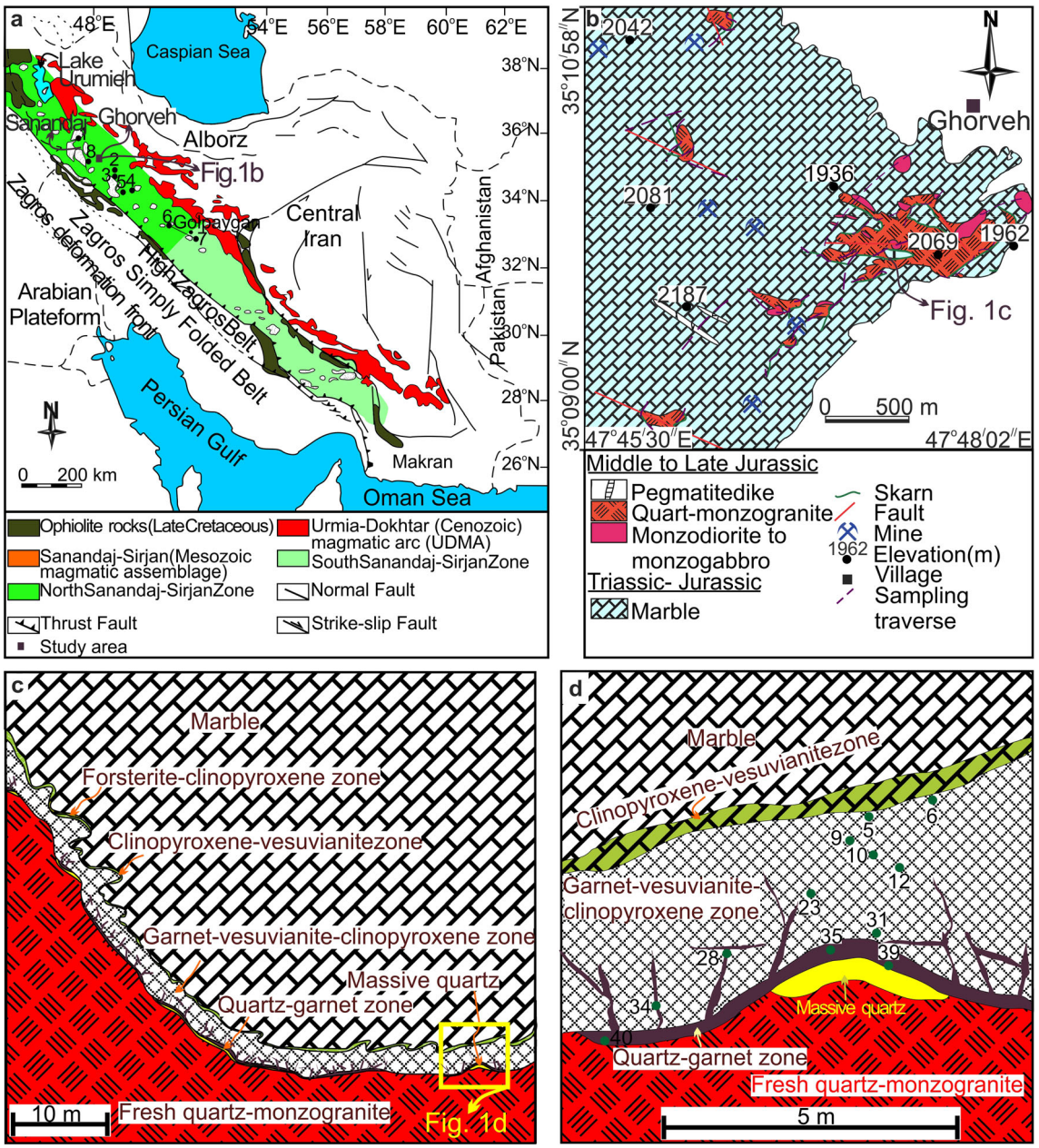

Fig. 1 **a** Simplified tectonic map of Iran showing the Sanandaj–Sirjan zone (SSZ) (modified from Dilek et al. 2010; Mohajjel et al. 2003) and occurrence and distribution of metallic mineralizations associated with Late Jurassic intrusions. Study area is within the quadrangle in the west of the map. Localities codes: 1, Zafar-Abad, Fe; 2, Hamedan Galali, Baba-Ali and Hamekasi, Fe; 3, Shams-Abad, Fe; 4, Dehe-Hossein, W-Sn ± Cu; 5, Nezam-Abad, W-Sn ± Cu; 6–7, Malayer-Isfahan, Pb-Zn; 8, Ebrahim-Attar tungsten skarn. **b** Detailed geologic map of the Ghorveh-Seranjic (GS) skarn showing host rocks, intrusive bodies, dikes and skarn localities. Modified from a geologic map of the Ghorveh by Hosseini, 1999. **c** Detailed interpretative map of the GS skarn showing zonation patterns. **d** Composition changes map in garnet within quartz-garnet and garnet-vesuvianite-clinopyroxene zones from the GS skarn. Numbers indicates the maximum subcalcic component (spessartine+almandine) in garnet at various green points

content; i.e., the actual mineral content is given in volume%. The modal analysis was performed using a Zeiss Axioplan research microscope. Based on optical microscopic observations, sixteen polished-thin sections with representative calc-silicate minerals (e.g. garnet, vesuvianite, clinopyroxene) from the GS skarn were selected for electron probe microanalyser (EPMA). EPMA analyses were obtained using a Cameca SX-50. Mineral compositions were determined by wavelength dispersive X-ray spectrometery (WDX) analysis for all measured elements. The system's five WDS spectrometers were equipped with PET, LIF, PET, TAP and TAP crystals. Operating conditions were as follows: acceleration voltage of 15 kV, beam current of 15 nA, and beam diameter of 10 μm (to avoid light element migration) for vesuvianite,

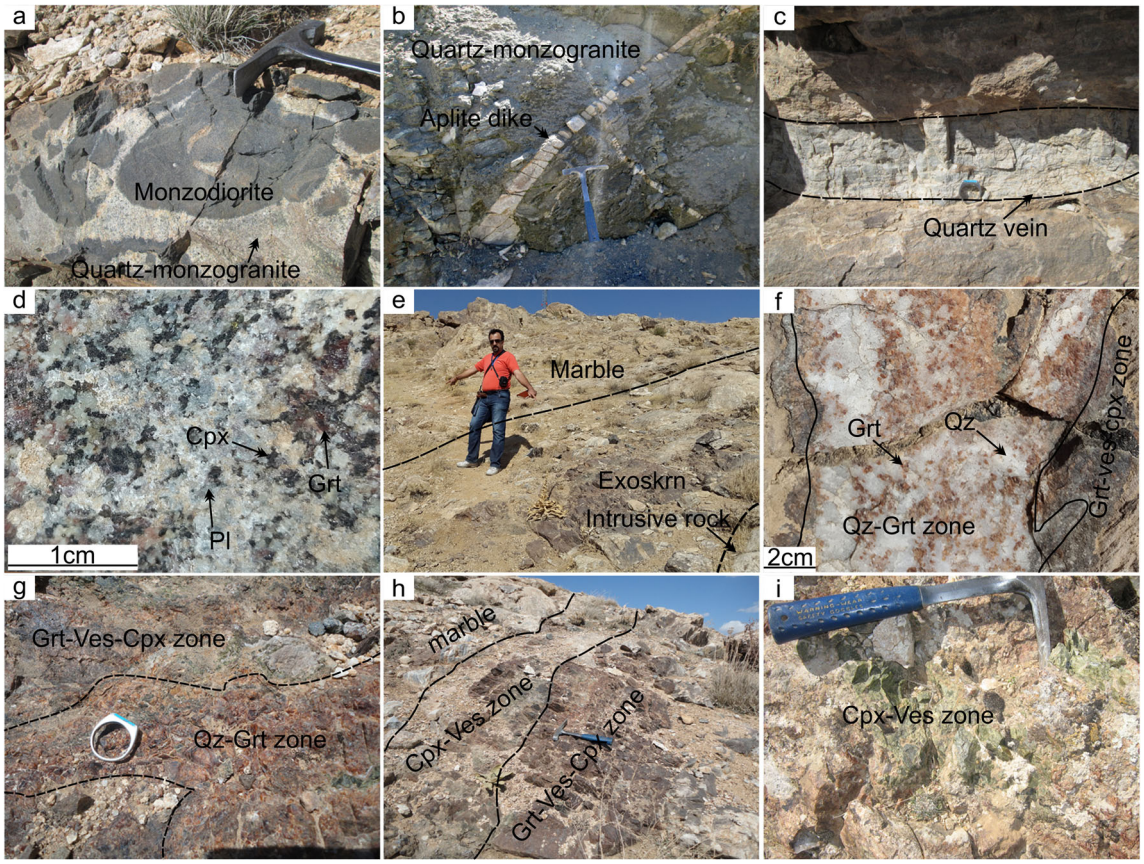

Fig. 2 Exposures of intrusive and skarn rocks. **a** rounded/elliptical shaped mafic microgranular enclaves of monzodiorite within quartz monzogranite (view to the east); **b** leucogranite aplite dikes crosscut the plutonic rocks (view to the northeast); c) quartz vein crosscut the pluton toward the skarn contact (view to the northeast); **d** fine-grained crystals of clinopyroxene, garnet, plagioclase in hand sample of typical endoskarn zone; **e** exoskarn zone occurs as lenses at the contact of the pluton and the marble (view to the north); **f** quartz-garnet zone occurs as veinlet within garnet-vesuvianite-clinopyroxene zone, containing quartz and garnet (view to the east); **g-i** Outcrop features of exoskarn zones. Abbreviations: Cpx = clinopyroxene, Grt = garnet, Ves = vesuvianite, Qz = quartz, Pl = plagioclase

epidote and amphibole and 1 μm for clinopyroxene, garnet and scheelite. Acquisition times were selected as 20 s on peak and 10 s on each background. Calibration standards were albite (Na), orthoclase (K), corundum(Al), wollastonite (Ca, Si), periclase (Mg), rutile (Ti), rhodonite (Mn,), magnetite (Fe), chromium oxide (Cr), F-phlogopite (F), KCl (Cl), pure metal (W). The Kα lines were measured for all elements except for W (Mα) and data were reduced using the PAP procedure (Pouchou and Pichoir 1984-1985). R function (Arai 2010) and WinPyrox (Yavuz 2013) programs were used to recast garnet and pyroxene analyses in order to estimate ferric and ferrous iron and end-member components of garnet and clinopyroxene following a normative calculation. Selected analytical results are presented in Tables 1 to 6. Mineral abbreviations are from Whitney and Evans (2010). Chemical formula and end-member proportions for the minerals were calculated by using the Deer et al. (1992) method.

Major element analyses of the fresh nine samples were performed using a PANalytical Axios Advanced X-ray fluorescence (XRF) on fused glass beads, composed of sample material and lithium borate flux of 1:5 ratio, in order to eliminate mineralogical effects and reduce inter-element effects. Trace and rare earth elements (REEs) were analyzed using an Agilent 7700 x inductively coupled plasma-mass spectrometry (ICP-MS), following lithium meta-borate fusion and HNO_3 total digestion. The analytical error for most elements is less than 2%. The detection limit for trace elements and REEs analysis is 0.01 to 0.1 ppm. ArcMap software was used for calculating the area of the GS skarn zones.

Petrography and mineral assemblage of skarn zones

The GS skarn is heterogeneous and coarse-grained with an internal zoning. The principal skarn minerals are garnet, clinopyroxene, vesuvianite, amphibole, epidote, quartz, and calcite together with scheelite, chlorite, titanite, pyrrhotite, pyrite, chalcopyrite and apatite as subordinate or accessory minerals. Based on the relictic textures of the protoliths, both endo- and exoskarn zones are developed in the GS skarn. Endoskarn is limited, while exoskarn is widespread in the area.

Endoskarn occurs as a narrow zone of 2 to 15 cm width restricted to the southwestern contact with medium- to fine-grained granular granite texture (Fig. 2d). It is composed of prograde minerals (e.g. clinopyroxene, plagioclase and garnet), retrograde minerals (e.g. epidote, amphibole and sericite) (Fig. 3a) and minor amounts of residual minerals from the intrusion (e.g. orthoclase, apatite and pyrite). Garnet is locally developed by replacement of primary igneous minerals, particularly plagioclase, and its abundance increases toward the exoskarn zone. Plagioclase crystals are commonly associated with apatite showing distinct sericitization. Clinopyroxene occurs as dark green and fine-grained crystals replacing the original mafic minerals of the quartz-monzogranite intrusion.

Exoskarn zones occur as lenses within the marble in the GS intrusion border with a sharp contact. Four different mineral assemblages were recognized based on morphological, mineralogical and textural relationship of mineral assemblages; quartz-garnet, garnet-vesuvianite-clinopyroxene, clinopyroxene-vesuvianite and forsterite-clinopyroxene (Fig. 1c and b-i).

The forsterite-clinopyroxene zone rarely occurs along the boundary between the marble and clinopyroxene-vesuvianite zone as a partially narrow border zone. Its thickness varies from 1 to 40 cm and comprises less than 2% of the skarn. The zone is recognized by calcite-dolomite (20–60 vol%), forsterite (10–30 vol%), diopsidic clinopyroxene (5–10 vol%), brucite (2–5 vol%) and serpentine (2–5 vol%) mineral assemblage showing mainly granoblastic texture of various grain size (<0.1–10 mm). Forsterite mainly occurs as fine-grained, subhedral to euhedral homogeneous crystal of <0.6 mm in length. Type Ib clinopyroxene occurs as a light green fine- to coarse-grained, subhedral to euhedral, short-

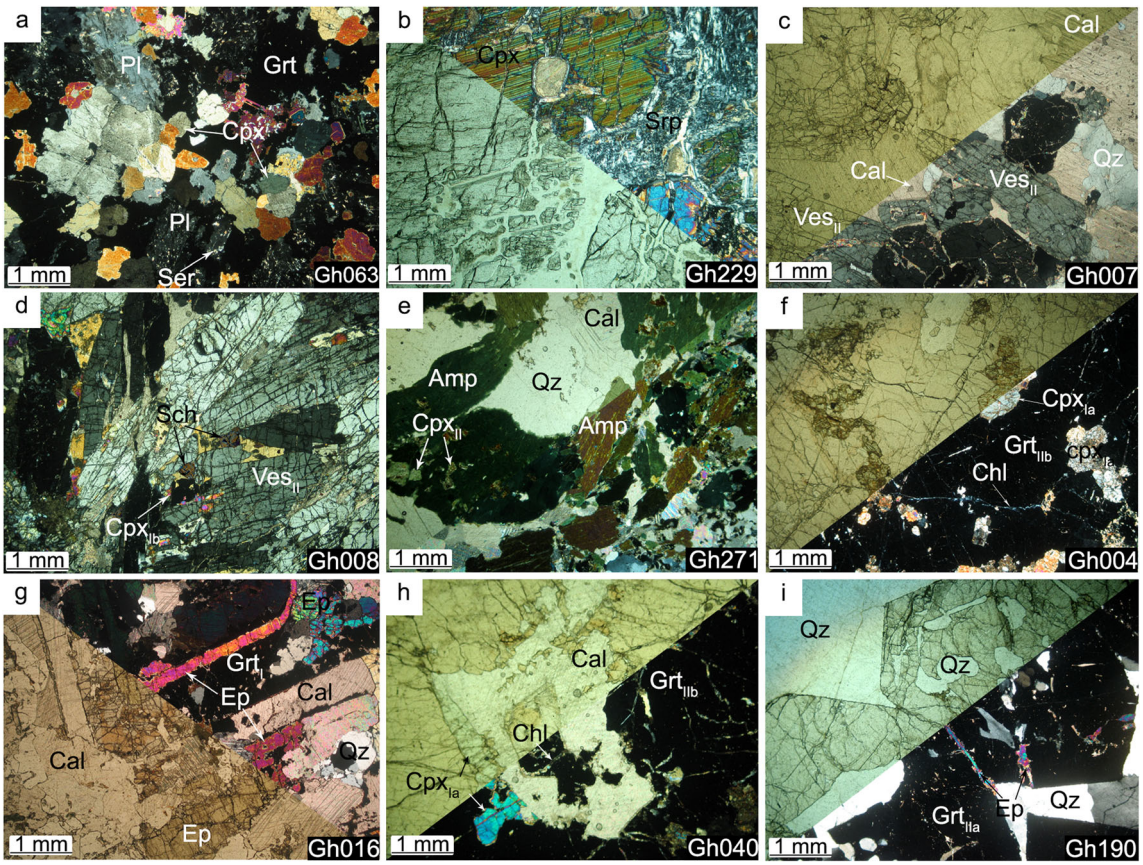

Fig. 3 Photomicrographs of the mineral assemblages and their textural properties in the endoskarn (a), clinopyroxene-forsterite zone (b), clinopyroxene-vesuvianite zone (c-e), garnet-vesuvianite-clinopyroxene zone f-h) and quartz-garnet zone (i). a) clinopyroxene, garnet and plagioclase crystals in XPL; b) serpentinization resulting from clinopyroxene alteration, Diagonal upwards in XPL and diagonal downwards in PPL; c) vesuvianite porphyroblasts in the marble, Diagonal upwards in PPL and diagonal downwards in XPL; d) clinopyroxene replaced by vesuvianite and increasing vesuvianite and scheelite abundance toward the marble front in XPL; e) replacing of clinopyroxene by amphibole and nematoblastic texture in XPL; f) garnet poikiloblasts consist of relict clinopyroxene, Diagonal upwards in PPL and diagonal downwards in XPL; g) epidotic filaments within part of type I garnet, Diagonal upwards in XPL and diagonal downwards in PPL; h) replacement of clinopyroxene by chlorite and calcite, Diagonal upwards in PPL and diagonal downwards in XPL; i) epidote crystals filling open-spaces between type IIa garnets in a quartz matrix, Diagonal upwards in PPL and diagonal downwards in XPL. Abbreviations: Cpx = clinopyroxene, Grt = garnet, Ves = vesuvianite, Qz = quartz, Pl = plagioclase, Ser = sericite, Srp = serpentine, Cal = calcite, Amp = amphibole, Sch = scheelite, Ep = epidote, Chl = chlorite

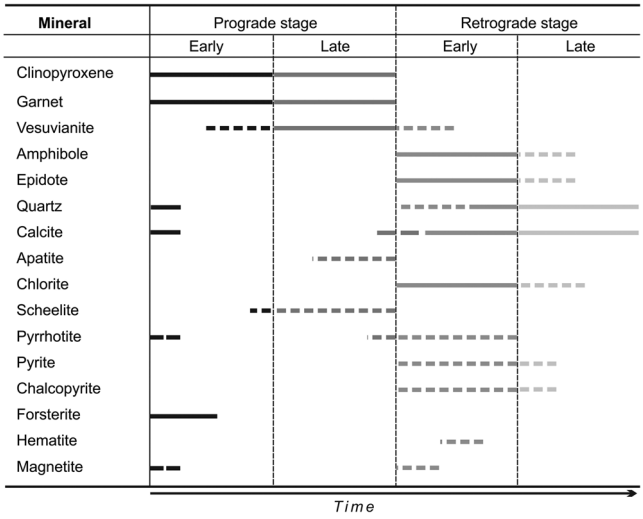

Fig. 4 Schematic diagram showing paragenetic relationships of mineral assemblages in the GS skarn zones, based on paragenetic relation and microtextural data

prismatic crystals (0.2 mm to 10 mm in diameter). Brucite and serpentine are common products of retrograde alteration formed around and within fractures in clinopyroxene and forsterite crystals (Fig. 3b).

The clinopyroxene-vesuvianite zone mostly crops out as the outer zone of the GS skarn. Its thickness varies from 0.1 to 1 m and comparises less than 15% of the GS skarn. It is a light- to dark-green rock with a granoblastic, poikiloblastic and porphyroblastic texture composed of vesuvianite (30–70 vol%), calcite (10–40 vol%), clinopyroxene (10–30 vol%), quartz (5–10 vol%) and scheelite (0.5–1 vol%). The ratio of clinopyroxene to vesuvianite is less than 1:2. Type I vesuvianite is formed as felted masses, anhedral crystals, khakish-yellow replacing interstitial clinopyroxene with scheelite in the calcite matrix. Type II vesuvianite is green-gray in color, showing various sizes and textures and often forms coarse tabular and/or prismatic, subhedral-euhedral, up to 5 mm long porphyroblastic crystalswithin the marble matrix (Fig. 3c). Scheelite is present as fine-grained (<0.2 mm), subhedral to anhedral, homogeneous, colorless to white crystals, mainly intergrown with clinopyroxene and vesuvianite (Fig. 3d) and scheelite is mainly associated with vesuvianite (Fig. 4). Clinopyroxene occurs in subhedral to euhedral short prismatic, slightly light-green (type I) or brownish-green (type II) crystals with a grain size ranging from 0.2 to 4 mm. Clinopyroxene is index mineral of the prograde stage of GS skarn and exhibits a granoblastic texture. Insignificant (<1 vol%) fine-grained flattened wedge-shaped titanite crystals were found as relictic inclusions in the prograde clinopyroxene. Calcite is present as fine- to coarse-grained rhombohedral crystals (<0.1–2 mm) forming the matrix. Retrograde alteration of the zone includes replacement of

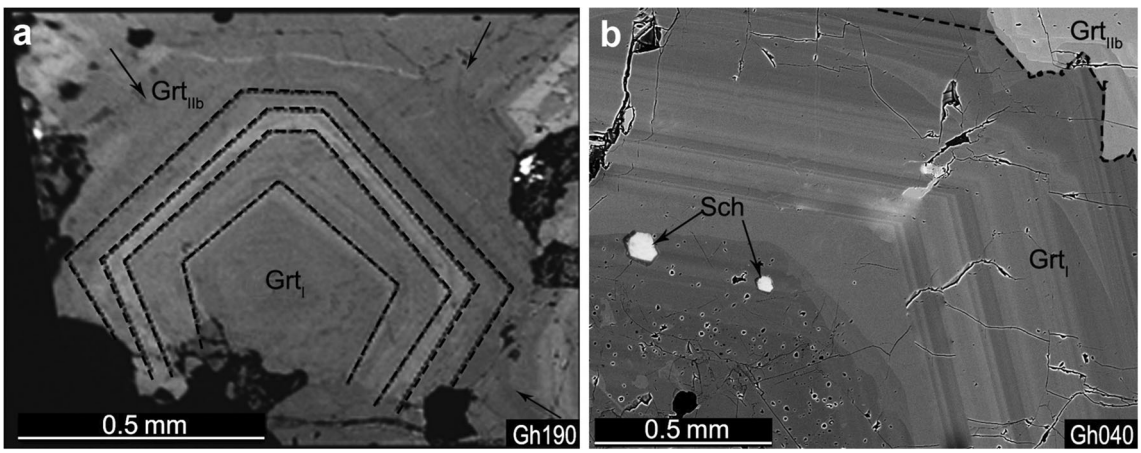

Fig. 5 Back-scattered electron (BSE) images from the GS skarn garnets: **a** epitaxial growth of type II*b* garnet with oscillatory zoning on preexisting garnet (type I) in the garnet-vesuvianite-clinopyroxene zone; **b** Zoning of type *I* garnet with replacing or interstitial scheelite in the garnet-vesuvianite-clinopyroxene zone. Abbreviations: Grt = garnet; Sch = scheelite

Table 1 Representative chemical compositions, and calculated mineral formulae and end-member fractions for garnet in exoskarn zones

Zones	Garnet-vesuvianite-clinopyroxene skarn												Quartz- garnet skarn								
Sample no.	Gh-190	Gh-190	Gh-190	Gh-88	Gh-88	Gh-88	Gh-64	Gh-64	Gh-14	Gh-14	Gh-190	Gh-190	Gh-44	Gh-44	Gh-24	Gh-24	Gh-10	Gh-51	Gh-51	Gh-48	Gh-45
Position	1b	1d	1 g	1a	1d	1 g	1a	1c	2d	2f	1a	1c	1a	1d	1a	1b	2c	1a	1d	1a	1e
Type	I	I	I	I	I	I	I	I	IIb	IIb	IIb	IIb	IIa	IIa	IIa	IIa	IIa	IIa	IIa	IIa	IIa
Oxides (wt%)																					
SiO_2	37.55	37.61	37.03	38.54	37.47	37.64	37.52	37.54	37.85	37.70	37.37	37.02	39.45	39.50	39.25	39.51	39.16	39.35	38.85	39.41	39.58
TiO_2	0.37	0.35	0.19	0.18	0.01	0.33	0.02	0.05	0.12	0.10	0.26	0.28	0.05	0.00	0.01	0.03	0.01	0.02	0.00	0.02	0.04
Al_2O_3	15.98	15.34	14.92	16.12	13.24	12.39	17.16	16.28	16.68	16.86	17.87	18.18	25.29	23.93	24.06	24.02	24.26	24.01	23.74	24.23	22.46
Cr_2O_3	0.01	0.08	0.00	0.02	0.02	0.00	0.00	0.00	0.06	0.00	0.01	0.00	0.00	0.06	0.01	0.03	0.01	0.03	0.10	0.00	0.17
FeO^*	10.15	10.68	12.41	8.84	11.95	13.14	12.83	13.13	12.24	15.19	13.46	13.26	11.35	13.87	13.45	13.13	12.99	13.03	13.21	13.14	15.42
MnO	3.61	3.56	4.52	2.86	2.72	3.65	1.66	1.71	6.41	6.65	8.39	8.29	0.45	1.06	0.80	1.01	0.97	1.02	1.05	1.02	1.31
MgO	0.05	0.04	0.04	0.03	0.05	0.07	0.00	0.04	0.10	0.15	0.10	0.13	0.13	0.06	0.08	0.09	0.07	0.09	0.08	0.06	0.17
CaO	31.86	32.07	29.74	32.58	32.00	30.58	30.63	30.94	27.04	23.92	22.20	22.23	23.09	20.96	22.01	21.67	21.83	22.19	22.00	22.04	20.48
Total	99.58	99.73	98.85	99.17	97.46	97.80	99.82	99.69	100.50	100.57	99.66	99.39	99.81	99.45	99.68	99.49	99.30	99.75	99.02	99.92	99.63
Calculated mineral formulae (apfu)**																					
Si	2.94	2.95	2.94	3.01	3.00	3.02	2.95	2.96	2.96	2.97	2.97	2.95	2.99	3.03	3.01	3.02	3.00	3.01	3.00	3.01	3.06
Ti	0.02	0.02	0.01	0.01	0.00	0.02	0.00	0.00	0.01	0.01	0.02	0.02	0.00	0.00	0.00	0.00	0.00	0.00	0.00	0.00	0.00
Al	1.47	1.42	1.40	1.48	1.25	1.17	1.61	1.54	1.54	1.56	1.67	1.70	2.26	2.16	2.17	2.17	2.19	2.16	2.16	2.18	2.04
Cr	0.00	0.00	0.00	0.00	0.00	0.00	0.00	0.00	0.00	0.00	0.00	0.00	0.00	0.00	0.00	0.00	0.00	0.00	0.01	0.00	0.01
Fe^{3+}	0.56	0.61	0.65	0.51	0.75	0.81	0.38	0.44	0.49	0.46	0.35	0.33	0.00	0.00	0.00	0.00	0.00	0.00	0.00	0.00	0.00
Fe^{2+}	0.10	0.09	0.18	0.07	0.05	0.07	0.46	0.43	0.31	0.54	0.55	0.55	0.72	0.89	0.86	0.84	0.83	0.83	0.85	0.84	1.00
Mn	0.24	0.24	0.30	0.19	0.18	0.25	0.11	0.11	0.42	0.44	0.56	0.56	0.03	0.07	0.05	0.07	0.06	0.07	0.07	0.07	0.09
Mg	0.01	0.00	0.00	0.00	0.01	0.01	0.00	0.00	0.01	0.02	0.01	0.02	0.01	0.01	0.01	0.01	0.01	0.01	0.01	0.01	0.02
Ca	2.67	2.69	2.53	2.72	2.75	2.63	2.58	2.61	2.27	2.02	1.89	1.90	1.87	1.72	1.81	1.78	1.79	1.82	1.82	1.80	1.70
Total	8.02	8.02	8.02	7.99	8.00	7.97	8.09	8.09	8.01	8.01	8.01	8.02	7.88	7.89	7.91	7.89	7.90	7.91	7.92	7.90	7.91
Calculated nominal end-member fractions (mol%)																					
Grossular	60.56	58.39	52.36	65.68	54.31	47.80	67.92	66.84	51.07	44.13	45.04	46.27	70.94	63.89	66.14	65.86	66.45	66.54	65.83	66.40	60.07
Andradite	28.55	31.04	32.78	25.47	37.47	41.11	19.54	22.46	24.75	23.42	17.46	16.85	0.00	0.00	0.00	0.00	0.00	0.00	0.00	0.00	0.00
Pyrope	0.00	0.00	0.00	0.12	0.20	0.28	0.00	0.16	0.00	0.00	0.00	0.00	0.53	0.25	0.34	0.39	0.29	0.39	0.33	0.24	0.70
Almandine	1.68	1.31	3.98	2.34	1.79	2.42	8.79	6.63	9.33	18.02	17.76	17.16	27.28	33.10	31.58	31.20	30.89	30.55	31.01	30.92	35.61
Spessartine	8.08	7.96	10.30	6.33	6.17	8.39	3.75	3.90	14.31	14.14	18.92	18.86	1.10	2.56	1.90	2.43	2.32	2.41	2.49	2.43	3.08

FeO^* = total iron content

** Calculated based on 12 oxygen atoms per formula unit

clinopyroxene by an amphibole±chlorite+carbonate±hematite mineral assemblage (Fig. 3e).

The garnet-vesuvianite-clinopyroxene zone is composed dominantly of garnet, vesuvianite and clinopyroxene and minor amounts of scheelite, calcite, quartz and sulfides (pyrrhotite and chalcopyrite). Garnet-vesuvianite-clinopyroxene zone is the most widespread of all these zones and makes up approximately 75% of the GS skarn. This zone is recognized with its brownish-green color in hand specimen, by its granoblastic, poikiloblastic texture under the microscope. The mineral assemblage of this zone is composed of garnet (50–70 vol%), vesuvianite (10–30 vol%), clinopyroxene (2–20 vol%), calcite (up to 5 vol%), quartz (up to 2 vol%), scheelite (up to 1 vol%) and pyrrhotite (up to 1 vol%). Garnet is the most abundant mineral in this zone and occurs as a prograde stage mineral (Fig. 4) with euhedral to anhedral shape. Subhedral garnet shows its best features toward the intrusion, especially those associated with quartz veins. At least two prominent populations of garnets are distinguished in hand specimens and thin sections based on their optical and textural relationship. The early prograde-stage (type I) garnet is brownish to blackish-red in color, coarse-grained, poikiloblastic, euhedral to subhedral, and typically anhedral in shape when associated with quartz and calcite inclusions. The textural evidence shows grossular-rich garnet (type I) and clinopyroxene (type Ia) are formed contemporaneously. The late prograde-stage (type IIb) garnets are pale to moderately reddish-brown, anhedral and/or occurs as overgrowths on preexisting garnets and/or between type I garnets. Type IIb garnets contain clinopyroxene (type Ia) relicts (Fig. 3f) and are typically anisotropic associated with epitaxial growth with oscillatory zoning on preexisting garnets (Fig. 5a). Scheelite is rare and is mainly formed as disseminated and sporadic crystals in type I garnet (Fig. 5b). Two distinct vesuvianite generations were identified in hand specimens and thin sections. In detail, type I vesuvianite forms relict in type IIb garnet, while type II vesuvianite occurs as porphyroblastic crystals that crosscut the late prograde garnet and contains relicts of type Ia clinopyroxene. Epidotization and carbonatization are the main alteration processes that occurred in the garnet-vesuvianite-clinopyroxene zone (Fig. 3g). Retrograde minerals such as amphibole, epidote, chlorite, quartz and calcite are commonly overprinting the garnet-vesuvianite-clinopyroxene zone (Fig. 3g–h).

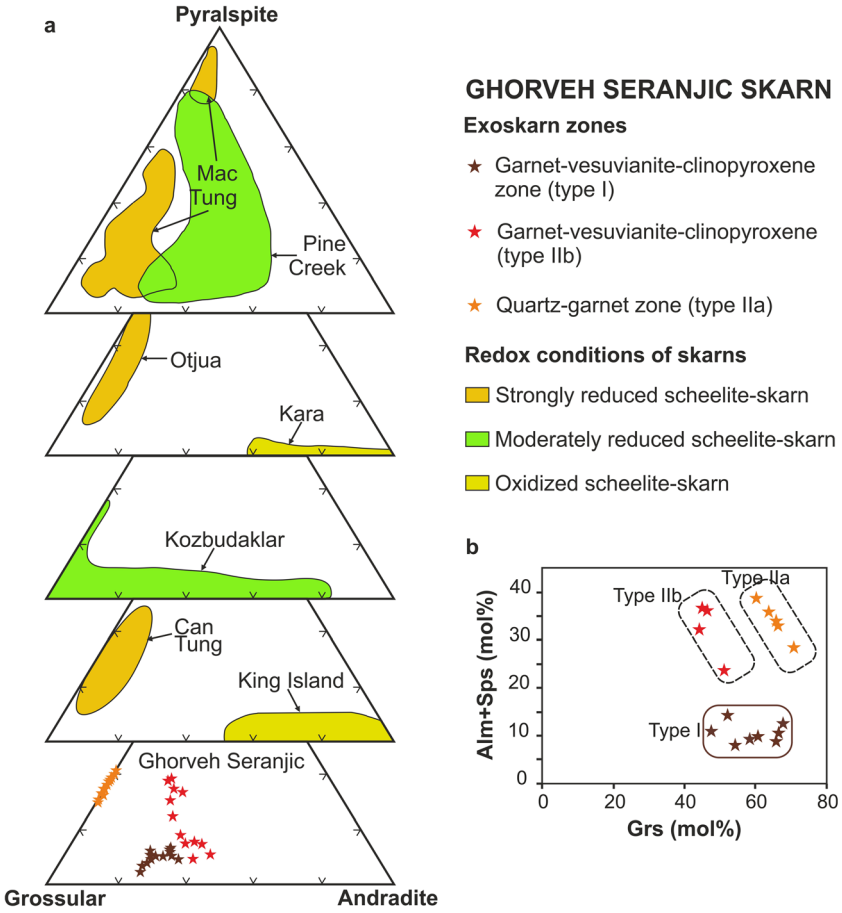

Fig. 6 **a** Ternary diagrams showing compositional variation of garnet from the GS skarn and garnet data from other scheelite-bearing skarn of different redox conditions (MacTung, Canada from Dick and Hodgson 1982; Pine Creek, California from Newberry 1982; Otjua, Namibia from Steven and Moore 1994; Kara, Tasmania from Zaw and Singoyi 2000; Kozbudaklar, Turkey from Orhan 2017; CanTung from Khin Zaw 1976; King Island, Tasmania from Kwak and Tan 1981). Representative EPMA data from the GS skarn are given in Table 1; **b** almandine+spessartine *vs.* grossular diagram of the GS garnet

Table 2 Representative chemical compositions, and calculated mineral formulae and end-member fractions for clinopyroxene in endo-exoskarn zones

Zone	Garnet-vesuvianite-clinopyroxene zone					Vesuvianite-clinopyroxene zone									Forsterite-clinopyroxene zone						Endoskarn		
Sample no.	GR-07	Gh-75	Gh-75	Gh-193	Gh-64	Gh-187	Gh-187	Gh-184	G-08	G-08	G-08	G-08	Gh-193'	Gh- 204	Gh201	Gh-193	Gh-04	Gh-04	Gh-74	Gh-74	Gh-63	Gh-63	Gh-63
Position		1a	2c		2b	1a	1b	2c	1a	1b	2a	2b	1a			1a	1a	1c	1b	1c	4d	1b	1c
Type	Ia	Ia	Ia	Ia	Ia	Ia	Ia	II	II	II	II	II	Ib	II	Ib	Ib	Ib	Ib	Ib	Ib	Ia	Ia	Ia
Oxides (wt%)																							
SiO_2	48.73	48.35	49.05	49.02	49.63	48.75	48.59	51.08	51.05	51.06	51.32	51.34	51.56	51.56	49.98	49.98	50.53	50.58	51.52	51.60	48.98	49.26	49.20
TiO_2	0.04	0.01	0.00	0.05	0.00	0.04	0.00	0.04	0.05	0.00	0.00	0.00	0.00	0.00	0.00	0.00	0.02	0.01	0.00	0.00	0.02	0.00	0.00
Al_2O_3	0.35	0.27	0.44	0.47	0.24	0.44	0.46	0.37	0.34	0.34	0.29	0.28	0.49	0.49	0.51	0.51	0.47	0.30	0.31	0.27	0.42	0.31	0.31
Cr_2O_3	0.00	0.01	0.00	0.00	0.04	0.01	0.02	0.00	0.00	0.00	0.00	0.00	0.00	0.00	0.00	0.00	0.04	0.00	0.00	0.00	0.03	0.00	0.00
FeO*	20.06	19.39	20.32	20.57	19.97	20.33	20.34	14.96	11.13	10.97	11.06	11.01	14.01	14.01	13.66	13.66	12.95	12.95	11.79	11.19	23.33	22.55	22.77
MnO	3.02	2.83	2.78	2.37	3.01	3.12	2.66	2.69	0.82	0.89	0.85	0.97	2.22	2.22	2.37	2.37	2.09	2.43	2.20	2.11	1.43	0.88	0.90
MgO	4.59	5.52	4.59	4.74	5.27	4.56	4.66	7.73	10.47	10.18	10.65	10.67	8.17	8.17	8.54	8.54	9.01	9.21	9.84	10.43	3.00	3.80	3.76
CaO	22.47	21.76	22.06	21.92	21.44	22.24	22.10	22.88	24.39	24.21	24.55	24.63	23.30	23.30	23.75	23.75	23.61	23.75	24.10	24.61	23.18	23.28	22.88
Na_2O	0.19	0.26	0.24	0.23	0.32	0.17	0.31	0.17	0.16	0.24	0.18	0.15	0.33	0.33	0.24	0.24	0.27	0.19	0.00	0.03	0.27	0.24	0.30
K_2O	0.00	0.00	0.01	0.00	0.00	0.00	0.01	0.00	0.03	0.00	0.00	0.02	0.01	0.01	0.00	0.00	0.00	0.01	0.11	0.13	0.00	0.01	0.00
Total	99.74	98.78	99.71	99.58	100.14	99.95	99.49	99.97	98.61	98.01	99.10	99.27	100.08	100.15	99.39	99.05	99.00	99.44	99.86	100.36	100.64	100.34	100.11
Calculated mineral formulae (apfu)**																							
Si	1.95	1.95	1.96	1.96	1.97	1.95	1.95	1.99	1.97	1.98	1.97	1.97	2.00	1.99	1.95	1.96	1.97	1.97	1.98	1.97	1.97	1.96	1.97
Ti	0.00	0.00	0.00	0.00	0.00	0.00	0.00	0.00	0.00	0.00	0.00	0.00	0.00	0.00	0.00	0.00	0.00	0.00	0.00	0.00	0.00	0.00	0.00
Al	0.02	0.01	0.02	0.02	0.01	0.02	0.02	0.02	0.02	0.02	0.01	0.01	0.02	0.02	0.02	0.02	0.02	0.01	0.01	0.01	0.02	0.01	0.01
Cr	0.00	0.00	0.00	0.00	0.00	0.00	0.00	0.00	0.00	0.00	0.00	0.00	0.00	0.00	0.00	0.00	0.00	0.00	0.00	0.00	0.00	0.00	0.00
Fe^{3+}	0.09	0.11	0.07	0.06	0.07	0.09	0.10	0.01	0.05	0.04	0.06	0.06	0.02	0.02	0.10	0.10	0.07	0.09	0.04	0.07	0.08	0.08	0.08
Fe^{2+}	0.58	0.54	0.61	0.62	0.60	0.59	0.58	0.47	0.31	0.32	0.30	0.29	0.43	0.43	0.34	0.35	0.35	0.33	0.33	0.28	0.70	0.67	0.69
Mn	0.10	0.10	0.09	0.08	0.10	0.11	0.09	0.09	0.03	0.03	0.03	0.03	0.07	0.07	0.08	0.08	0.07	0.08	0.07	0.07	0.05	0.03	0.03
Mg	0.27	0.33	0.27	0.28	0.31	0.27	0.28	0.45	0.60	0.59	0.61	0.61	0.47	0.47	0.50	0.50	0.53	0.54	0.57	0.60	0.18	0.23	0.22
Ca	0.97	0.94	0.95	0.94	0.91	0.95	0.95	0.95	1.01	1.01	1.01	1.01	0.97	0.96	0.99	1.00	0.99	0.99	0.99	1.01	1.00	0.99	0.98
Na	0.01	0.02	0.02	0.02	0.02	0.01	0.02	0.01	0.01	0.02	0.01	0.01	0.03	0.02	0.02	0.02	0.02	0.01	0.01	0.00	0.02	0.02	0.02
K	0.00	0.00	0.00	0.00	0.00	0.00	0.00	0.00	0.00	0.00	0.00	0.00	0.00	0.00	0.00	0.00	0.00	0.00	0.00	0.01	0.00	0.00	0.00
Total	4.00	4.00	4.00	4.00	4.00	4.00	4.00	4.00	4.00	4.00	4.00	4.00	4.01	4.00	4.00	4.03	4.02	4.03	4.01	4.02	4.02	4.00	4.00
$Fe/(Mg + Fe^{2+})$	0.68	0.62	0.69	0.69	0.66	0.69	0.68	0.51	0.34	0.35	0.33	0.32	0.48	0.48	0.41	0.41	0.40	0.38	0.37	0.32	0.79	0.75	0.75
Fe/(Fe + Mn)	0.85	0.85	0.87	0.89	0.85	0.85	0.87	0.84	0.92	0.92	0.92	0.90	0.86	0.86	0.81	0.81	0.83	0.80	0.83	0.80	0.93	0.96	0.96
Mn/Fe	0.18	0.18	0.15	0.13	0.17	0.18	0.16	0.19	0.09	0.09	0.09	0.11	0.16	0.17	0.23	0.23	0.20	0.24	0.21	0.25	0.07	0.04	0.04
Calculated nominal end-member fractions (mol%)																							
Di	27.33	33.27	27.21	27.87	31.15	27.18	28.02	43.46	57.11	55.91	57.85	57.99	43.67	45.78	49.20	44.94	47.65	48.02	51.12	53.35	16.31	21.67	21.56
Hd	58.20	54.25	60.68	61.41	59.58	59.38	58.34	45.84	29.10	30.40	28.14	27.67	48.65	42.22	34.23	47.06	44.46	44.80	40.72	38.02	75.02	64.73	65.98
Jo	14.47	12.48	12.11	10.72	9.27	13.45	13.63	10.70	13.79	13.70	14.01	14.34	7.67	12.01	16.57	8.00	7.89	7.18	8.16	8.64	8.67	13.60	12.46

FeO* = total iron content

** Calculated based on 6 oxygen atoms per formula unit

The quartz-garnet zone is closest to the intrusive body and occurs as a narrow, 1 cm to 0.5 m wide zone (Fig. 2f–g). Boundary between the quartz-garnet and garnet-vesuvianite-clinopyroxene zones is gradual in quartz-garnet veinlets (Fig. 2c–d), extending from the intrusion toward the garnet-vesuvianite-clinopyroxene zone. It is recognized by a mineral assemblage of garnet (10–50 vol%), quartz (5–80 vol%), and vesuvianite (up to 10 vol%) with porphyroblastic to granoblastic textures. Garnet is observed as single coarse-grained (≥2 cm in diameter) crystals, light red to orange in color (type IIa garnet), within the quartzitic matrix near the intrusion (Fig. 3i). Quartz is fine- to medium-grained, subhedral to anhedral. Quartz typically occurs in small veins or veinlets that crosscut earlier mineral assemblages of the retrograde alteration stage. There is no scheelite in this zone. Coarse-grained euhedral garnet occurs within each vein. In the retrograde stage, fractures in garnets are filled by epidote, quartz, calcite and chlorite. Epidote rarely develops filling the vugs between coarse-grained garnets with a granoblastic texture. Chlorite is a retrograde alteration product of garnet and occurs as a very fine-grained (<0.1 mm), sheet-like crystals at rims and fractures of garnet.

Results

Mineral chemistry of garnet

The compositional variation of the GS skarn garnets is given in Table 1 and plotted on a grossular-andradite-pyralspite ternary diagram together with other scheelite skarn deposits with different redox conditions as reference (Fig. 6a).

EPMA data show that the GS garnets from three distinct clusters (Fig. 6a) are dominated by grossular and some andradite and pyralspite (Table 1). Type I garnet has a grossular-andradite composition (of $Grs_{65.68}$ $And_{25.47}$ to $Grs_{47.80}$ $And_{41.11}$) with spessartine ($Sps_{6.17–10.30}$) and almandine ($Alm_{1.31–3.98}$), collectively less than 15% (Table 1). Type II garnet has a subcalcic composition between grossular-pyralspite with intensely varying andradite proportions. Type II garnet is a grossular-andradite-pyralspite (of $Grs_{44.13}$ $And_{23.42}$ $Pyr_{32.16}$ to $Grs_{51.07}$ $And_{24.75}$ $Pyr_{23.64}$) and a grossular-pyralspite (of $Grs_{70.94}$ $Pyr_{28.38}$ to $Grs_{60.07}$ $Pyr_{38.68}$) in the garnet-vesuvianite-clinopyroxene and quartz-garnet zones, respectively. Type I garnet has been found in most scheelite

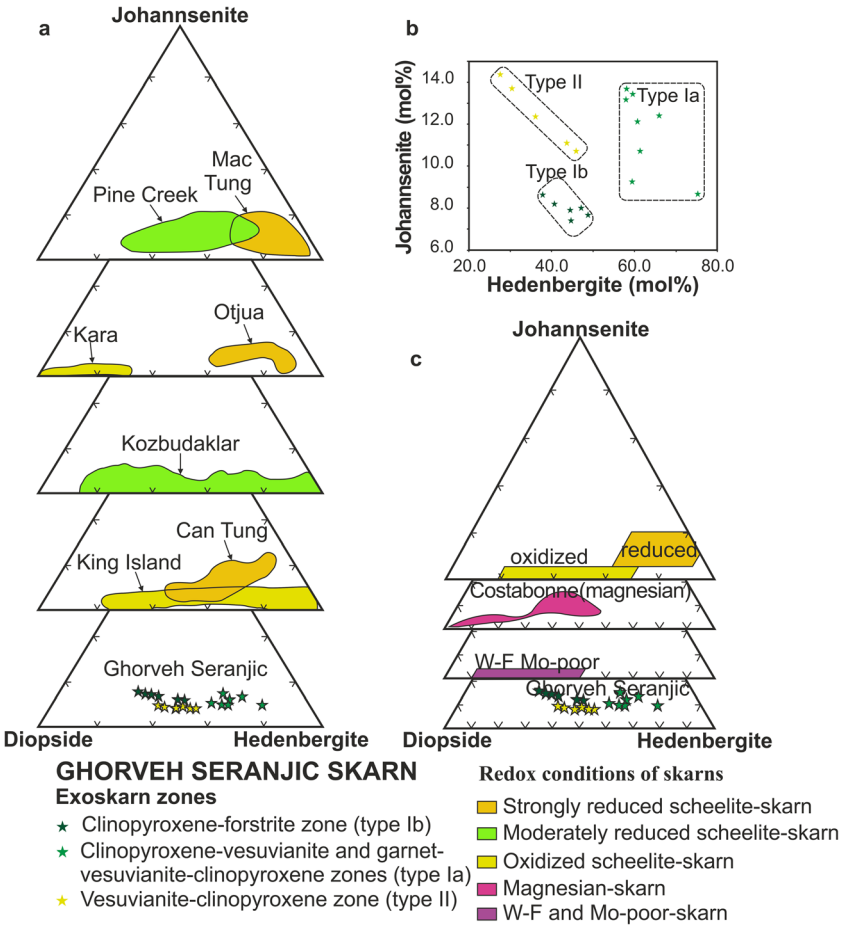

Fig. 7 **a** Ternary diagrams showing compositional variation of clinopyroxene from the GS skarn and clinopyroxene data from other scheelite-bearing skarn of different redox conditions (MacTung, Canada from Dick and Hodgson 1982; Pine Creek, California from Newberry 1982; Otjua, Namibia from Steven and Moore 1994; Kara, Tasmania from Zaw and Singoyi 2000; Kozbudaklar, Turkey from Orhan 2017; CanTung from Khin Zaw 1976; King Island, Tasmania from Kwak and Tan 1981). Representative EPMA data from the GS skarn are given in Table 2; **b** johannsenite *vs.* hedenbergite diagram of clinopyroxene from the GS skarn; c) Clinopyroxene composition from the GS skarn, compared to those of "oxidized," "reduced," and Costabonne (magnesian) W skarns (Einaudi et al. 1981) and from W-F Mo-poor skarn (Newberry 1998)

Table 3 Representative chemical compositions and calculated mineral formulae of vesuvianite in exoskarn zones

Zones	Vesuvianite-clinopyroxene zone				Garnet-vesuvianite-clinopyroxene zone			
Sample no.	Gh-148	Gh-148	Gh-231	Gh-231	Gh-08	Gh-08	Gh-241	Gh-241
Position	4b	4c	2b	3a	2a	2b	1a	1d
Type	I	I	I	II	I	I	II	II
Oxides (wt%)								
SiO_2	36.41	36.25	37.37	36.09	37.66	37.42	37.17	36.55
TiO_2	0.07	0.01	0.08	0.13	0.15	0.12	0.04	0.05
Al_2O_3	17.36	17.50	17.35	17.61	17.69	17.48	19.13	18.40
Cr_2O_3	0.01	0.02	0.00	0.00	0.00	0.00	0.01	0.02
FeO*	5.28	5.07	4.31	5.38	3.72	3.92	5.80	6.15
MnO	0.42	0.53	0.60	0.77	0.37	0.49	1.33	1.91
MgO	1.23	1.27	1.49	0.93	1.52	1.57	0.07	0.06
CaO	36.93	36.94	35.53	36.46	35.46	35.94	34.67	34.29
Na_2O	0.08	0.06	0.13	0.06	0.09	0.08	0.04	0.02
K_2O	0.00	0.00	0.01	0.01	0.00	0.00	0.04	0.01
F	1.64	2.05	2.07	1.87	1.79	2.00	1.62	1.57
Cl	0.04	0.08	0.08	0.03	0.08	0.06	0.04	0.03
Total	99.46	99.78	99.01	99.35	98.54	99.08	99.96	99.05
Calculated mineral formulae (apfu)**								
Si	17.96	17.98	17.87	17.99	17.93	18.05	17.85	18.05
Al	9.90	9.84	10.11	9.80	9.75	9.84	9.89	9.82
Mg	1.77	1.71	1.72	1.92	1.76	1.66	1.84	1.89
Fe	1.39	1.46	1.43	1.38	1.40	1.50	1.44	1.35
Ca	18.47	18.53	18.34	18.42	18.75	18.38	18.57	18.35
Mn	0.11	0.10	0.10	0.10	0.11	0.09	0.12	0.09
F	3.49	3.15	3.22	3.62	3.03	2.87	3.35	2.77
Cl	0.39	0.35	0.39	0.33	0.37	0.31	0.35	0.35
OH	5.12	5.51	5.39	5.05	5.60	5.82	5.30	5.88
Total	58.60	58.60	58.57	58.61	58.70	58.53	58.70	58.54
Mg/Fe	1.27	1.17	1.20	1.39	1.26	1.11	1.28	1.40

FeO* = total iron content

** Calculated based on 76 oxygen atoms per formula unit

skarn deposits (Einaudi et al. 1981; Newberry 1982; Fonteilles et al. 1989; Timon Sanchez et al. 2009; Orhan 2017). The composition of type I and IIb garnets in the garnet-vesuvianite-clinopyroxene zone represent a wide range from grossular to andradite and show an evolution similar to those of Pine Creek and Kozbudaklar skarns. The composition of type IIa garnet in the quartz-garnet zone shows a similar evolution to those of Otjua and Cantung skarns (Fig. 6a). The subcalcic garnets without andradite (type IIa) in the quartz-garnet zone convert to less subcalcic toward the marble front and finally becomes dominantly subcalcic garnet with andradite (type IIb) in the garnet-vesuvianite-clinopyroxene zone (Fig. 1d). The grossular *vs.* almandine+spessartine proportion displays a constant correlation in type I garnet and a negative correlation in type IIa, b garnets (Fig. 6b). The composition of garnets (type I and IIb) in the garnet-vesuvianite-clinopyroxene zone are more andradite-rich than type IIa garnet in the quartz-garnet zone. The grossular content of type IIa garnet in the quartz-garnet zone increase with slightly increasing manganese and ferrous iron, indicating that the skarn-forming fluid may have changed during the skarn evolution (Orhan 2017). Mg, Cr and Ti contents are very low in all the GS skarn garnets and their content is overally less than 0.02 apfu (atoms per formula). Very low content of TiO_2 in the garnet crystals of the GS skarn implies a much larger activity of SiO_2 during their hydrothermal formation

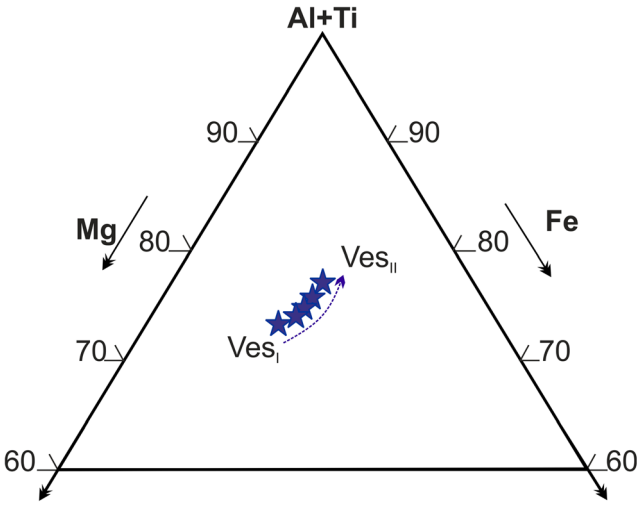

Fig. 8 Chemcial compositions (based on EPMA results) of vesuvianite from the GS skarn, plotted in terms of Fe + Mg + (Al + Ti) = 100 mol%. Each point represents one analysis. Representative EPMA data from the GS skarn are given in Table 3. Abbreviations: Ves_I = type I vesuvianite, Ves_{II} = type II vesuvianite

(Dingwell and Brearley 1985). These low values allow a clear differentiation between skarn garnets (Table 1) and igneous garnets in general (Dingwell and Brearley 1985).

Mineral chemistry of clinopyroxene

EPMA data of clinopyroxene from the various skarn zones of the GS skarn are given in Table 2. The compositional variation is plotted in the diopside-hedenbergite-johansenite ternary diagram together with other scheelite skarn deposits with different redox conditions (Fig. 7a). Generally, each single crystal of clinopyroxene is almost homogeneous, although there are variations between crystals. The GS skarn clinopyroxene has high Fe/Fe + Mn ratios (0.80–0.96), Cr_2O_3, TiO_2, and Na_2O contents. Significantly lower contents of Cr, Ti, and Na indicate that the origin of clinopyroxenes is metamorphic (Berger et al. 2005). Early prograde clinopyroxene is predominantly composed of hedenbergite (type Ia) ($Hd_{58.18–75.02}$ $Di_{28.66–16.31}$ $Jo_{13.16–8.67}$) and diopside (type Ib) ($Hd_{38.02–48.65}$ $Di_{53.35–43.67}$ $Jo_{8.64–7.67}$) in endoskarn, (garnet-vesuvianite-clinopyroxene and clinopyroxene-vesuvianite) and (forsterite-clinopyroxene and garnet-vesuvianite-clinopyroxene) exoskarn zones, respectively. Late prograde type II clinopyroxene has an intermediate composition between hedenbergite and diopside ($Hd_{27.67–45.84}$ $Di_{57.99–43.46}$ $Jo_{14.33–10.70}$) in clinopyroxene-vesuvianite and forsterite-clinopyroxene zones (Fig. 7b) with a slight increase of the johansenite component. Manganese enrichment in clinopyroxene is a common process during the late prograde substage of calcic tungsten-bearing skarns (Einaudi et al. 1981; Steven and Moore 1994; Orhan 2017). Type Ia clinopyroxene is present as relictic inclusion in type IIb garnet and type I vesuvianite in the garnet-vesuvianite-clinopyroxene zone. Type II clinopyroxene occurs with granoblastic texture in vesuvianite-clinopyroxene and forsterite-clinopyroxene zones.

Type Ib clinopyroxene in the forsterite-clinopyroxene zone is compatible with clinopyroxene from magnesian skarns, such as Costabonne deposit (Fig. 7c) and oxidized skarns (e.g. King Island), while type Ia clinopyroxene with hedenbergite-enrichment in clinopyroxene-vesuvianite and garnet-vesuvianite-clinopyroxene zones indicate a moderately reduced to moderately oxidized environment in the early

Table 4 Representative chemical compositions and calculated mineral formulae of amphibole in exoskarn zones

Sample no.	Gh-88	Gh-88	Gh-272	Gh-272	Gh-14	Gh-14
Position	4a	4b	1c	1d	2a	2b
Oxides (wt%)						
SiO_2	43.05	41.51	44.49	41.31	40.53	40.74
TiO_2	0.18	0.18	0.23	0.22	0.28	0.26
Al_2O_3	9.19	10.48	8.06	10.90	12.21	12.01
FeO*	23.34	23.94	22.43	25.52	25.65	25.89
MnO	1.33	1.45	1.74	1.24	1.45	1.53
MgO	7.09	6.33	7.60	5.52	3.32	3.52
CaO	11.50	11.33	11.47	11.37	11.76	11.53
Na_2O	1.51	1.63	1.55	1.60	1.69	1.69
K_2O	1.13	1.60	0.72	0.99	1.53	1.69
F	0.70	0.76	0.78	0.12	0.89	0.92
Cl	0.01	0.09	0.10	0.14	0.12	0.11
Cr_2O_3	0.00	0.00	0.00	0.00	0.00	0.00
Total	99.03	99.32	99.17	98.94	99.43	99.89
Calculated mineral formulae (apfu)**						
Si	6.57	6.58	6.75	6.32	6.37	6.36
Al ^{iv}	1.43	1.42	1.25	1.68	1.63	1.64
Al ^{vi}	0.22	0.29	0.19	0.29	0.63	0.57
Ti	0.02	0.03	0.03	0.03	0.03	0.03
Cr	0.00	0.00	0.00	0.00	0.00	0.00
Fe^{3+}	0.75	0.58	0.69	0.94	0.16	0.31
Fe^{2+}	2.23	2.48	2.15	2.32	3.21	3.07
Mn	0.17	0.19	0.22	0.16	0.19	0.20
Mg	1.61	1.44	1.72	1.26	0.78	0.82
Ca	1.88	1.85	1.86	1.86	1.98	1.93
Na	0.45	0.48	0.46	0.47	0.51	0.51
K	0.22	0.31	0.14	0.19	0.31	0.34
F	0.34	0.37	0.38	0.06	0.44	0.45
Cl	0.00	0.02	0.02	0.04	0.03	0.03
OH	1.66	1.61	1.60	1.90	1.53	1.52
Total	17.55	17.65	17.46	17.53	17.80	17.78
$Mg/(Mg + Fe^{2+})$	0.42	0.37	0.44	0.35	0.20	0.21
$Fe^{3+}/(Fe^{3+}+Al^{vi})$	0.77	0.67	0.79	0.77	0.20	0.35

FeO* = total iron content

** Calculated based on 24 oxygen atoms per formula unit

prograde stage such as King Island, Cantung and Pine Creek scheelite skarns (Fig. 7 a, c).

Type II clinopyroxene in the vesuvianite-clinopyroxene zone is similar to clinopyroxene from the Pine Creek scheelite deposit, which characterizes a moderately reduced environment. The hedenbergite to johansenite proportion of early and late clinopyroxene in the clinopyroxene-bearing zones of the GS skarn show two clusters (Fig. 7b). In spite of the narrow range of johansenite, type Ib diopside-rich clinopyroxene and type II clinopyroxene show a negative correlation between the hedenbergite and johansenite components (Fig. 7b). Similar negative hedenbergite-johansenite correlations are reported toward the granitic rocks, from the Sargipali scheelite skarn in India (Chowdhury and Lentz 2011) and the Kozbudakhlar scheelite skarn in Turkey (Orhan 2017). Type Ia hedenbergite-rich clinopyroxene shows a constant correlation between the hedenbergite and johansenite components. The comparison between considerably magnesium-rich clinopyroxene (early) and slightly manganese-rich clinopyroxene (late) indicate that the skarn-forming fluid changed during the skarn evolution.

Mineral chemistry of vesuvianite

Chemical analyses of the GS vesuvianite are presented in Table 3. In general, each single crystal of vesuvianite is almost homogeneous, though there are insignificant compositional variation between crystals. The optical and textural characteristics of vesuvianite show a clear correspondence with chemical oscillations. Late vesuvianite tends to have consistently low magnesium concentrations (Fig. 8), in averaging around 0.08 wt% MgO. The manganese content is very low (0.37–1.91 wt% MnO) with an average of 0.80 wt% MnO. The fluorine content in vesuvianite is high (1.57–2.07 wt% F), which is a common phenomenon in formation of vesuvianite as a dominant calc-silicate mineral and is quite compatible with other W-F-Sn skarns (Jahns 1944; Kwak and Askins 1981; Dobson 1982). The chlorine content is very low, <0.08 wt%. Type I vesuvianite is present as relictic inclusion in type II garnet, developed during the late prograde substage, in the garnet-vesuvianite-clinopyroxene zone. Type II vesuvianite occurs as poikiloblastic crystals with relictic inclusion of clinopyroxene in the early retrograde stage of vesuvianite-clinopyroxene and garnet-vesuvianite-clinopyroxene zones.

Mineral chemistry of amphibole

EPMA data indicate that amphiboles of the GS skarn are calcic (Table 4), falling sporadically into the hastingsitic and ferro-edenitic hornblende fields (Leak 1978; Fig. 9a). The manganese to Fe/Fe + Mg proportion of amphibole from the GS skarn displays a relatively negative correlation, which is similar to the GS skarn clinopyroxene, and shows a systematic Mn enrichment (Fig. 9b). Elevated F content in amphibole (0.12–0.92 wt%) as well as in vesuvianite (1.57–2.07 wt%) is reflecting an enrichment of F in the volatile phase during the scheelite-bearing hydrous skarn formation (Gaspar and Inverno 2000; Zaw and Clark 1978; Newberry et al. 1997). These fluorine values are common in W and Sn skarns and are similar to those reported in amphiboles from Riba de Alva (Gasper and Inverno 2000) and Cantung E-zone skarns (Zaw and Clark 1978) (Fig. 9c). Low

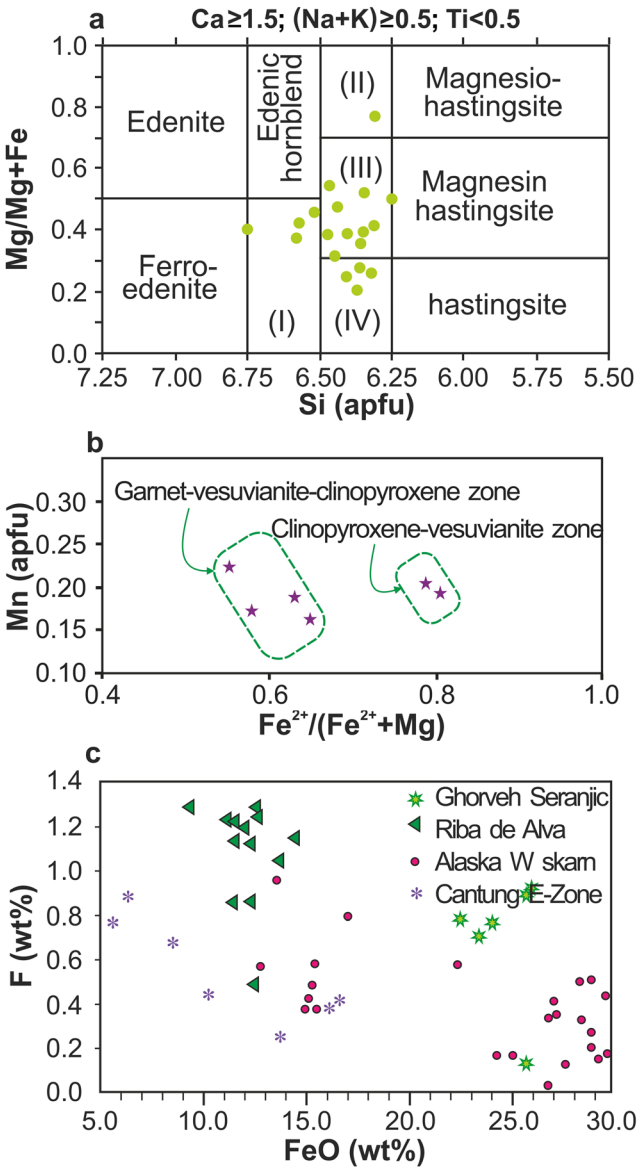

Fig. 9 a) Plot of Mg/(Mg + Fe) against Si of amphibole classification criteria of Leak (1978). I = ferro-edentic hornblende, II = magnesio-hastingsitic hornblende, III = magnesian hastingsitic hornblende, IV = hastingsitic hornblende; b) Mn versus $Fe^{2+}/(Fe^{2+}+Mg)$ of amphibole from the GS skarn; c) F versus FeO diagram of amphibole from the GS skarn, compared to those from the Cantung E zone (Zaw and Clark 1978); Alaskan W skarns (Newberry et al. 1997); Riba de Alva scheelite skarn (Gaspar and Inverno 2000); d) Compositions of epidote from the GS skarn

chlorine content (0.01–0.14) is similar to the other hydrous minerals of the GS skarn.

Mineral chemistry of epidote

Representative analyses of epidote from the various skarn zones are given in Table 5. The pistacitic component (Ps = $Fe^{3+}/(Fe^{3+}+Al^{VI})$ of the GS skarn zones is in the range of 0.21 to 0.30 (Table 5, Fig. 9d), and fits to the aluminum-enriched clinozoisite subgroup with the mineral species of 'epidote' (Armbruster et al. 2006).

Mineral chemistry of scheelite

Chemical analyses of scheelite from the GS skarn are given in Table 6. The calculated powellite content is very low (Pw% < 7%). and there is no chemical zoning in each single crystal of scheelite. The paragenetic and textural relations between the prograde anhydrous minerals indicate that this low-Mo scheelite formed during the prograde alteration. Low-Mo scheelite is typical of scheelite formed during retrograde alteration (Gaspar and Inverno 2000). Mo-rich scheelite formed during prograde alteration in many oxidized tungsten skarns (Einaudi et al. 1981; Kwak 1987; Newberry 1998).

Discussion

Conditions of the GS skarn formation

Petrological and textural studies of mineral assemblages in the GS skarn show that skarn evolution occurred in four stages (Fig. 4). Stage I and II mineral assemblages are dominated by anhydrous minerals i.e. clinopyroxene and garnet with different compositions, hydrous mineral (vesuvianite) and subordinate amounts of sulfide mineral (pyrrhotite). Scheelite mostly

Table 5 Representative chemical compositions and calculated mineral formulae of epidote in exoskarn zones

Sample no.	Gh-88	Gh-88	Gh-14	Gh-190	Gh-190	Gh-8	Gh-8	Gh-271
Position	1a	1c	3a	1a	1d	2b	1a	1c
Oxides (wt%)								
SiO_2	37.96	38.08	37.79	37.91	38.08	38.37	38.59	37.80
TiO_2	0.14	0.08	0.17	0.14	0.15	0.29	0.05	0.05
Al_2O_3	21.53	21.84	21.78	22.61	23.08	23.43	24.96	21.97
Cr_2O_3	0.00	0.06	0.02	0.00	0.00	0.00	0.00	0.00
FeO*	12.76	12.91	12.79	12.51	12.40	11.99	9.12	12.31
MnO	0.61	0.40	0.68	1.00	0.67	0.53	0.23	0.42
MgO	0.01	0.02	0.03	0.03	0.03	0.04	0.05	0.01
CaO	23.09	22.88	22.40	22.65	23.04	23.27	23.28	22.84
Na_2O	0.00	0.02	0.02	0.00	0.00	0.01	0.16	0.01
K_2O	0.00	0.00	0.00	0.00	0.01	0.00	0.02	0.00
Total	96.10	96.28	95.67	96.84	97.45	97.92	96.44	95.40
Calculated mineral formulae (apfu)**								
Si	3.05	3.05	3.05	3.02	3.01	3.02	3.05	3.05
Ti	0.01	0.00	0.01	0.01	0.01	0.02	0.00	0.00
Al	2.04	2.06	2.07	2.12	2.15	2.17	2.32	2.09
Cr	0.00	0.00	0.00	0.00	0.00	0.00	0.00	0.00
Fe^{3+}	0.86	0.86	0.86	0.83	0.82	0.79	0.60	0.83
Mn	0.04	0.03	0.05	0.07	0.05	0.04	0.02	0.03
Mg	0.00	0.00	0.00	0.00	0.00	0.00	0.01	0.00
Ca	1.99	1.96	1.93	1.93	1.95	1.96	1.97	1.98
Na	0.00	0.00	0.00	0.00	0.00	0.00	0.02	0.00
K	0.00	0.00	0.00	0.00	0.00	0.00	0.00	0.00
Total	7.99	7.98	7.98	7.99	7.99	7.99	8.00	7.98
$Al/(Al + Fe^{3+} + Cr)$	0.70	0.70	0.71	0.72	0.72	0.73	0.79	0.72
$Fe^{3+}/(Al + Fe^{3+})$	0.30	0.30	0.29	0.28	0.28	0.27	0.21	0.28

FeO* = total iron content

** Calculated based on 12.5 oxygen atoms per formula unit

Table 6 Representative chemical compositions and calculated mineral formulae of scheelite in exoskarn zones

Zone	Clinopyroxene-vesuvianite zone			Garnet-vesuvianite-clinopyroxene zone		
Sample no.	Gh-8	Gh-8	Gh-190	Gh-271	Gh-271	Gh-244
Position	1a	2d	3a	1a	4b	1a
Oxides (wt%)						
WO_3	79.46	78.24	80.01	78.96	79.01	79.32
CaO	19.47	19.83	20.03	19.96	19.49	19.39
Fe_2O_3	0.03	0.05	0.01	0.03	0.04	0.03
MoO_3	1.02	0.98	1.05	1.01	0.99	0.97
MgO	0.00	0.00	0.00	0.00	0.00	0.00
PbO	0.00	0.00	0.00	0.00	0.00	0.00
total	99.98	99.1	99.53	99.96	99.53	99.71
Calculated mineral formulae (apfu)*						
W	0.98	0.97	0.98	0.97	0.98	0.98
Ca	0.99	1.02	1.01	1.02	1.00	0.99
Fe	0.00	0.00	0.00	0.00	0.00	0.00
Mo	0.06	0.06	0.06	0.06	0.06	0.06
Mg	0.00	0.00	0.00	0.00	0.00	0.00
Pb	0.00	0.00	0.00	0.00	0.00	0.00
total	2.04	2.05	2.05	2.05	2.04	2.03
Mo/(Mo + W)	5.8	5.7	6.0	5.8	5.7	5.6

* Calculated based on 4 oxygen atoms per formula unit

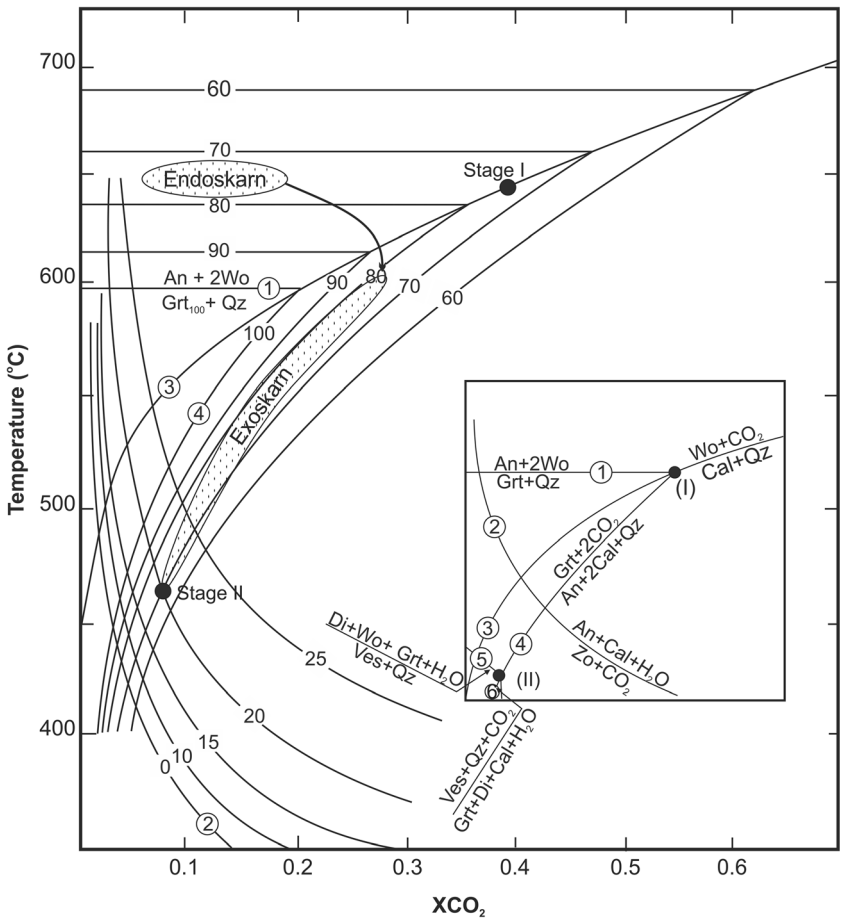

Fig. 10 Temperature-XCO_2 diagram in $p_{fluid} = 2$ kb showing the general environment of skarn evolution at the GS skarn (from endoskarn to exoskarn indicated by dotted area). The numbers on reaction (2) indicate mole % pistacite in epidote, whereas those for reactions (1) and (4) indicate mole% of grossular in grandite garnets. gr_{100} is pure Ca-Al garnet (grossular) $gr_{20–80}$ are andradite-grossular solid solution. Reactions from Newton (1966); Gordon and Greenwood (1971); Sweeney (1980). $XCO_2 = CO_2/(CO_2 + H_2O)$. Abbreviations: Grt = garnet, Ves = vesuvianite, An = anorthite, Qz = quartz, Wo = wolastonite, Cal = calcite, Di = diopside, Zo = zoisite, Chl = chlorite

occurs in stage I and II together with clinopyroxene and garnet. Abundance of scheelite slightly increases with vesuvianite development (Fig. 4). The stage III mineral assemblage is dominated by hydrous minerals i.e. vesuvianite, amphibole, epidote overprinting garnet and clinopyroxene. Additionally, pyrrhotite, pyrite and chalcopyrite as rare minerals developed only during stage III. The stage IV mineral assemblage consists of quartz and calcite typically in veins and veinlets cross-cutting stage III and earlier mineral assemblages.

The early prograde skarn stage with anhydrous minerals, such as garnet and clinopyroxene, suggests a high temperature magmatic fluid origin (Kwak 1986; Meinert et al. 2003). Grossular-rich garnet (type I) composition together with primary euhedral quartz crystals, minor anorthite and the absence of wollastonite in the endoskarn mineral assemblages indicate the upper temperature limit of the skarn formation (T = 630 °C, 2 kbar) based on the reaction Gr + Qz = An+2Wo (Fig. 10, reaction 1). The calculated equilibration temperatures using the garnet-clinopyroxene Fe^{2+}-Mg geothermometer of Ravna (2000) showed that the anhydrous mineral assemblage (stage I) formed between 530 °C to 620 °C at 2 kbar (Sheikhi et al. 2012). Grossular-bearing assemblages are indicative of low concentration of CO_2 during metamorphism (Le Anderson 1981; Deer et al. 1992), and the early anhydrous assemblages have fluid $XCO_2 \leq 0.4$. Shifts of the invariant intersection of the reactions Gr + Qz = An+2Wo and Gr + $2CO_2$ = An+2Cc + Qz (Fig. 10, reactions 1 and 4) are a function of the grossular component in garnet. These curves indicate that endoskarn formed at a temperature of ≤630 °C and $XCO_2 < 0.4$. Abundance of F-bearing minerals such as vesuvianite, instead of clinopyroxene, absence of wollastonite in the early prograde stage and also the mineral chemistry of hydrous minerals (Tables 3 and 4) suggest the presence of a F-rich fluid phase. The abundance of F in the hydrothermal system stabilizes vesuvianite even at higher CO_2 conditions (Dobson 1982), although, the absence of wollastonite and the occurrence of vesuvianite in the mineral assemblage are generally considered to be indicative of low XCO_2 conditions (Hochella et al. 1982). With time and due to temperature decrease, the lower temperature limit as well as the minimum XCO_2 of the prograde skarn assemblage is constrained based on epidote absence, which indicates a minimum temperature of ≈450 °C and a fluid composition of $XCO_2 < 0.1$.

Stability fields of dominant calcsilicate minerals in the GS skarn are a function of oxygen fugacity (fO_2), temperature (Fig. 11) and $CO_2/(CO_2 + H_2O)$ ratio or XCO_2 (Fig. 10). The (Fe,Mn)–Mg interdiffusion coefficient is strongly fO_2-sensitive (Dimanov and Wiedenbeck 2006). More oxidizing conditions would favor the formation of andradite and diopsidic clinopyroxene relative to hedenbergite (Gamble 1982; Gustafson 1974). Furthermore, grossular-rich garnet ($Grs_{60–70}$) requires lower fO_2 compare with andradite-rich ($Grs_{65–47}$ $And_{25–41}$) equivalents (Einaudi and Burt 1982). Clinopyroxene enrichment sequence of Mg–Fe–Mn is due to fluid depletion and temperature decrease (Capitani and Mellini 2000; Meinert 1987). The rarity of magnetite with garnet-quartz-hedenbergite-rich clinopyroxene suggests prograde skarn formation along a T- fO_2 path according to the reaction $9CaFeSi_2O_6$ (Hd) + $2O_2$ = $3Ca_3Fe_2Si_3O_{12}$ (And) + $9SiO_2$ (Qtz) + Fe_3O_4 (Mt) (Fig. 11, reaction 7 from Burton et al. 1982).

Formation of subcalcic garnet comparative to grandite garnet, indicates reducing conditions and more depth, which is compatible with field evidence and mineral chemistry data, i.e. as iron speciation of garnet changes with increasing distance from the intrusion, from ferric to ferrous garnet.

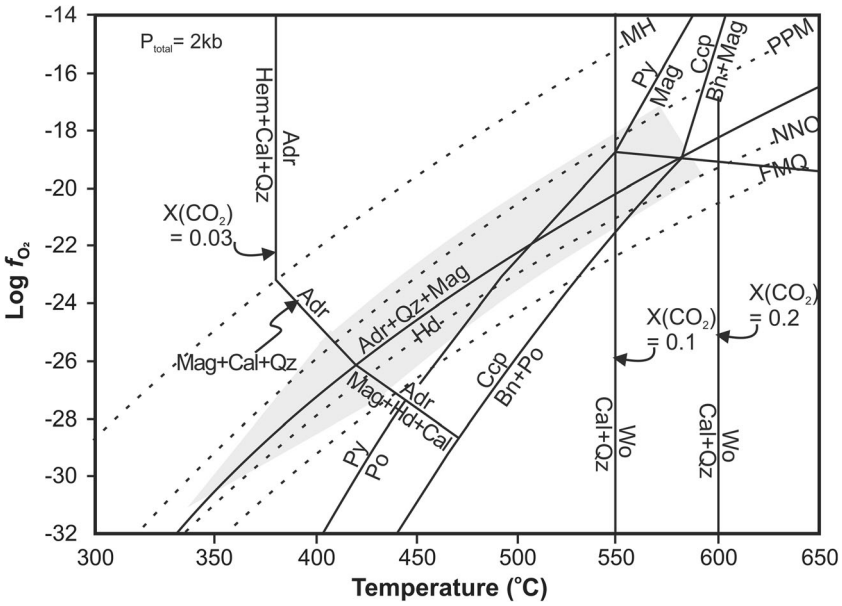

Fig. 11 Temperature-oxygen fugacity (fo_2) diagram at 2 kb showing the environment of the GS skarn formation (gray area), modified from Liou (1974). Reactions are from Greenwood (1967); Gordon and Greenwood (1971); Gustafson (1974). Abbreviations: Adr = andradite; An = anorthite; Hd = hedenbergite; Hem = hematite; Mag = magnetite; Ccp = chalcopyrite; Py = pyrite Po = pyrrhotite; Cal = calcite; Qz = quartz; Wo = wolastonite; NNO=Ni-NiO buffer; FMQ = Fayalite-Magnetite-Quartz buffer; PPM = pyrrhotite-pyrite-magnetite buffer; MH = magnetite-hematite buffer

Table 7 Major and trace element chemical compositions of the samples selected from the Ghorveh-Seranjic pluton

Sample	GH214	Gh145	FG287	Gh245	Gh 193	Gh212	Gh076	Gh064'	GH270
Oxides (wt%)									
SiO_2	75.07	76.27	75.27	78.47	76.14	74.32	74.76	71.12	76.74
TiO_2	0.01	0.02	0.20	0.05	0.04	0.03	0.02	0.67	0.06
Al_2O_3	13.12	13.45	11.68	11.22	13.67	13.98	14.12	10.12	13.07
$Fe_2O_3^*$	1.99	0.61	2.17	1.18	0.64	0.43	0.53	3.62	0.67
MnO	1.04	0.31	0.03	0.10	0.03	0.01	0.01	0.05	0.02
MgO	0.12	0.06	0.20	0.03	0.06	0.04	0.04	1.84	0.06
CaO	0.41	0.51	0.99	0.50	0.64	0.63	0.64	5.98	0.80
Na_2O	3.60	4.31	2.91	4.24	4.27	4.72	4.98	2.82	4.18
K_2O	4.50	4.05	5.33	3.73	3.89	5.03	4.81	2.13	4.12
P_2O_5	0.01	0.01	0.39	0.02	0.02	0.03	0.07	0.06	0.01
LOI	0.37	0.41	0.70	0.37	0.70	0.43	0.22	0.86	0.44
Total	100.24	100.01	99.87	99.91	100.10	99.65	100.20	99.27	100.16
Trace elements (ppm)									
V	5.45	3.20	23.00	16.0	5.72	1.15	17.14	112	3.80
Cr	214	37.2	63.0	245	46.1	71.3	45.4	105	251
Co	<1.3	3.99	3.00	3.00	<1.3	<1.3	5.04	9.58	<1.3
Ni	76.1	11.64	50.0	115	23.4	7.56	10.76	11.3	68.8
Cu	4.28	6.59	20.0	9.00	3.80	4.39	9.13	6.74	<0.4
Zn	9.68	3.27	87.0	54.0	4.03	4.03	2.37	52.6	8.82
Ga	18.8	nd	nd	nd	22.7	21.7	21.7	10.9	15.1
Rb	166	440	170	147	449	312	315	71.3	141
Sr	15.4	11.2	83.0	23.0	9.05	8.03	8.03	122	58.2
Zr	140	14	143	59.0	113	71.0	19.7	49.5	54.8
Nb	28.7	nd	20.0	50.0	32.1	28.1	68.0	8.1	18.95
Cs	2.1	11.7	nd	nd	11.2	2.64	2.06	<1.3	<1.3
Ba	26	25.2	303	10.0	26.0	3.97	1.20	224	77.2
Pb	16	1.6	107	113	10.0	15.1	14.94	5.97	16.1
Th	16	1.6	107	113	10.0	6.34	3.18	6.13	16.1
U	3	1.20	13.0	4.00	0.49	4.49	1.32	2.04	1.39
Hf	1	nd	nd	nd	nd	0.73	0.93	0.99	nd
Ta	2.39	2.90	nd	nd	2.90	3.79	4.35	0.23	nd
Y	280	5.30	68.0	92.0	5.70	4.61	10.9	14.1	5.75
La	8.68	4.50	nd	nd	3.10	0.47	0.92	18.7	4.48
Ce	12.9	5.60	58.0	31.0	<5.9	4.11	4.52	44.6	<5.9

Table 7 (continued)

Sample	GH214	Gh145	FG287	Gh245	Gh 193	Gh212	Gh076	Gh064'	GH270
Pr	0.52	0.57	0.15	0.51	0.57	0.24	0.51	5.0	1.12
Nd	11.7	2.90	0.57	2.21	4.31	0.92	1.86	14.3	5.50
Sm	0.67	0.63	0.63	1.02	0.61	0.33	1.32	2.96	1.32
Eu	0.01	0.01	0.01	0.01	0.01	0.00	0.01	0.58	0.01
Gd	0.95	0.53	0.17	0.74	0.53	0.28	0.99	3.12	1.45
Tb	0.12	0.11	0.14	0.19	0.13	0.11	0.57	0.51	0.19
Dy	1.33	1.20	0.24	0.38	0.98	0.56	3.41	3.09	1.42
Ho	0.20	0.21	0.02	0.15	0.19	0.14	0.23	0.47	0.20
Er	0.47	0.54	0.15	0.29	0.56	0.73	1.12	1.72	0.69
Tm	0.09	0.15	0.01	0.09	0.13	0.04	0.27	0.24	0.16
Yb	0.86	0.89	0.19	0.53	0.94	0.46	3.13	1.46	1.17
Lu	0.10	0.12	0.04	0.12	0.09	0.1	0.32	0.18	0.19
Rb/Sr	10.78	39.17	2.05	6.39	49.65	38.88	37.39	0.58	2.43

nd = not detected

* Total Fe as Fe_2O_3

Garnet with a significant almandine component ($alm_{25–35}$) forms only at an oxidation state along or below the Ni-NiO buffer. The increasing trend of a_{Fe} and Fe^{2+}–Mn^{2+} replacement in the grossularite garnet during the garnet precipitation is associated with a decrease in oxygen fugacity. The decrease in oxygen fugacity triggers scheelite deposition (Shimazaki 1977) causing an increase in the scheelite quantity in the late prograde stage. In addition, absence of graphite in the prograde skarn (exoskarn) assemblages provides a lower limit of oxygen fugacity, thus the GS skarn formed at temperatures between 580 to 400 °C and $\log fO_2 = -18$ to -28 (Fig. 11).

Geochemical evolution of the GS skarn

The GS skarn mineral assemblages are dominated by Ca-Al-Mg rich and Fe^{3+} poor minerals, though the Fe content of minerals increased during skarn evolution similar as reported in many other skarns (e.g. Pine Creek, Newberry 1982; Costabonne, Lummen and Verkaeren 1986). In the GS skarn, there is a Fe enrichment in skarn minerals with increasing proximity to the intrusion, suggesting that Fe, in addition to other components (Al, Si), was introduced into the skarn from the intrusive body.

The elemental composition trend of clinopyroxene in the GS skarn shows that type Ib clinopyroxene (the marginal zone) has the highest johannsenite amount, which is not compatible with typical Mn enrichment trends in the fluid phase. It seems that the wall rock composition (dolomitic marble) created an unusual increase of johannsenite. Type Ib and II clinopyroxene displays hedenbergite-johannsenite negative correlations, and an increase in hedenbergite with decreasing distance from the intrusive body. In general, the Mg:Fe:Mn proportions in the clinopyroxene of the skarn zones which reflects the local variations in wall rock-fluid and this is a common process during the prograde stage of scheelite-bearing skarn compatible with the fluctuation model of Nakano (1989, 1991). The Fe/Mg ratios of clinopyroxene reflect mostly the concentration of the components in the fluid phase rather than its oxidation state. The decrease of the Fe/Mg ratio in clinopyroxene with distance from hydrothermal conduits reflects increasing dolomitic component in the wall rock.

Garnet geochemical composition of the GS skarn indicates low MgO (<0.5) and variable Mn-Fe^{2+} and Fe^{3+} contents. The Fe^{2+}/Fe^{3+} ratio of garnets decreases with the increasing distance from the intrusion front, which is compatible with their Fe/Mn ratios. Type I and II garnet data show a decreasing trend in the Fe-Mn contents with distance from the intrusive body as Fe and Mn are supplied by hydrothermal fluid rather than by local dolomitic rocks (Chowdhury and Lentz 2011). The Fe/Mn ratio of GS garnet reflects depletion of Mn in fluid, as it precipitated Fe-rich and Mn-poor garnets near the intrusive front. The GS garnet compositions are not a simple

Table 8 Comparison of the GS skarn with other skarn occurrences

Features	GS[1]	Otjua[2]	King Island[3]	Kara[4]	CanTung[5]
Host rock	Early Jurassic Dolomitic marble	Late Proterozoic marble	Cambrian marble	Ordovician calcic marble	Cambrian calcic marble
Intrusion/age	Upper Jurassic monzogranite to granite	Highly fractionated Cambrian leucogranite	Devonian granite Devonian granite	Highly fractionated	Highly fractionated Cretaceous monzonite
Plumbing system	Via marble contact	Possibly via marble contact and fault	Via fault ± marble contact	Via marble contact	Via marble, contact
Zone of skarn development	Contact aureole	Contact aureole	Contact aureole	Contact aureole	Contact aureole
Prograde mineral assemblages	Fo + Cpx ± Qz ± Cal Grt + Cpx ± Ves ± Sch ±Qz ± Cal ± Ap		Grt + Cpx + Wo + Ves ±Sch Grt + Cpx ± Wo ± Ves ±Pl	Cpx + Grt + Sch ± Wo ± Ves ± Cal ± Qz ± An	
Retrograde mineral assemblages	Amp + Ep + Qz + Cal +Chl ± Ves	Amp + Bt + Ep + Chl ±Czo ± Fsp ± Cal	Qz + Cal + Amp + Ep + Chl + Bt ± Ap ± Fsp± Act±Zeo	Amp + Ep + Fsp + Qz +Cal + Sch + Chl ± Cpx ±Grt ± Ves	Amp + Bt + Qtz + Cal ± fl Czo ± Pl ± Ap
Pyrite	Minor	Minor	Abundant	Minor	Minor
Pyrrhotite	Abundant	Abundant	Minor	Absent	Abundant
Molybdenite	Nil	Minor	Minor	Absent	Minor
Magnetite	Minor	-?	Minor	Abundant	Nil
Early garnet composition	$Grs_{47–65}$, $(Adr_{25–41})$	$Grs_{43–79}$, $(Adr_{5–15})$	$Grs_{13–45}$, $(Adr_{43–98})$	$Grs_{0–25}$, $(Adr_{70–100})$	$Grs_{50–70}$, $(Adr_{30–50})$
Early pyroxene composition	$Hd_{38–75}$, $(Joh_{7–14})$	$Hd_{60–86}$, $(Joh_{4–11})$	$Hd_{41–88}$, $(Joh_{4–7})$	$Hd_{0–25}$, $(Joh_{2–3})$	$Hd_{75–100}$
Mo content in scheelite	$<Pow_7$	Absent	Mean Pow_{15}	$>Pow_{1–7}$	$<Pow_3$
Prograde temperatures	400 °C–580 °C		500–750 °C	349 °C–620 °C	450 °C–520 °C
Retrograde temperatures	183 °C–410 °C		300–405 °C	230–360 °C	270–400 °C
Confining pressure	<2 kbar	~3 kbar	1–2 kbar	1 kbar	2–3.8 kbar
Oxidation/reduction	Moderately reduced (to oxidized) (log $fO_2 = -18, -28$)	Reduced	Moderately oxidized	Very oxidized	Reduced

Features	Sangdong[6]	Los Santos[7]	Pine Creek[8]	Kozbudaklar[9]
Host rock	Cambrian limestone	Late Ordovician calcic marble	Upper Paleozoic calcic marble	Triassic calcic marble
Intrusion/age	Cretaceous granitoid (inferred)	Highly fractionated Permian biotite granite	Highly fractionated Upper Cretaceous	Eocene granodiorite
Plumbing system	Via fracture	Via marble contact	Via marble contact	Via marble contact
Zone of skarn development	Distal (500 m)	Contact aureole	Contact aureole	Contact aureole
Prograde mineral assemblages	Grt + Cpx + Wo ± Sch	Grt + Cpx + Aln + Sch + Ves + Wo	grt + cpx ± wo ± ves ± sc	Grt + Cpx ± Wo ± Ves ±Sch ± Qz ± Cal ± An± Sph ± Ap Grt + Cpx ± Wo ± Ves

Table 8 (continued)

				±Sch ± Qz ± Ap
Retrograde mineral assemblages		Grt + Cpx + Sch ± An±Ves ± Act ±Czo ± Ap ± Cal ± Qz ± Chl ± Ttn	Amp + Ep + Bt + Chl ± Cal+ Ap ± Pl ± Scp ± Fsp ± Sph ± Zo	Qz + Cal + Chl ± Ves ±Ep
Pyrite	Minor	Absent	Minor	Minor
Pyrrhotite	Abundant	Abundant	Minor	Minor
Molybdenite	Nil	Absent	Minor	Absent
Magnetite	Nil	Absent	Abundant	Minor
Early garnet composition	$Grs_{10–90}$, ($Adr_{10–100}$)	$Grs_{53–73}$, ($Adr_{37–44}$)	$Grs_{50–73}$, ($Adr_{20–46}$)	$Grs_{38–94}$, ($Adr_{0–61}$)
Early pyroxene composition	$Hd_{80–95, 3–25}$	$Hd_{82–87}$, ($Joh_{6–9}$)	$Hd_{40–57}$, ($Joh_{4–10}$)	$Hd_{61–96}$, ($Joh_{4–7}$)
Mo content in scheelite	<4% MoO_3	<Pow_1	~$Pow_{5–15}$	$Pow_{1–6}$, $Pow_{7–32}$
Prograde temperatures	Up to 600 °C	473 °C–519 °C	450 °C–550 °C	308 °C to ≥600 °C
Retrograde temperatures	300 °C	125–570 °C	305 °C–450 °C	101 °C–320 °C
Confining pressure	800 bar	2 kbar	1.5–2 kbar	2 kbar
Oxidation/reduction	Reduced (to moderately oxidized)	Reduced (to oxidized) (log fO_2 = −22, −29)	Moderately reduced (to oxidized) (log fO_2 = −22.5)	Moderately reduced (to oxidized) (log fO_2 = −22, −24)

[1] This study

[2] Steven and Moore (1994)

[3] Kwak and Tan (1981); Einaudi et al. (1981); Wesolowski and Ohmoto (1986); Wesolowski et al. (1988)

[4] Zaw and Singoyi (2000); Singoyi and Zaw (2001)

[5] Zaw (1976); Zaw and Clark (1978); Einaudi et al. (1981); Mathieson and Clark (1984); Rasmussen et al. (2011)

[6] Moon (1983)

[7] Timon Sanchez et al. (2009)

[8] Gray et al. (1968); Einaudi et al. (1981); Newberry (1982); Brown et al. (1985)

[9] Orhan (2017)

Abbreviations: Act = actinolite, Aln = allanite, Amp = amphibole, An = anorthite, Ap = apatite, Bt = biotite, Cal = calcite, Chl = chlorite, Cpx = clinopyroxene, Czo = clinozoisite, EP = epidote, Fsp = feldspar, Fo = forsterite, Grt = garnet, Pl = plagioclase, Qz = quartz, Sch = scheelite, Scp = scapolite, Sph = sphalerite, Tnt = titanite, Ves = vesuvianite, Wo = wolastonite, Zo = zoisite

function of distance from the intrusive body, but reflect rather the latest paths of fluid flow controlled by the host rock (Newberry 1983). Calcium activity decreases and iron-manganese activity increases towards the intrusion front causing subcalcic garnet and quartz precipitation. Distribution of scheelite in different garnet-bearing zones of the GS skarn shows that scheelite is soluble in the fluid where calcium activity is low. An increase in calcium activity close to the marble front triggered scheelite deposition. Therefore, subcalcic garnet and quartz assemblages can be used as hydrothermal fluid path and development of scheelite-bearing zone.

Textural evidence and mineral assemblages indicate that no tungsten minerals occurred during the early magnesian skarn and minor scheelite is mostly associated with iron-rich minerals (e.g. type Ia, II clinopyroxenes, type I, IIb garnets) formed during the late prograde phase similar to the King Island (Kwak and Tan 1981) and Southern Cordillera scheelite-bearing skarns (Newberry and Einaudi 1981) (Table 8).

Formation of highly pure scheelite in the GS skarn is due to reduced conditions as well as Mo-poor hydrothermal fluids. Generally, Mo-poor W-F skarns develop in association with peraluminous granites (Newberry et al. 1997; Newberry 1998). In addition, all those granitoids are highly fractionated, have high Rb/Sr ratios (Table 7) with water released relatively late in the crystallization history (Newberry and Swanson 1986; Meinert 1993), and are coarse-grained, have low W contents, lack hydrothermal alteration, and are commonly associated with pegmatite dikes (Meinert et al. 1980; Newberry and Einaudi 1981, Newberry and Swanson 1986, Newberry et al. 1997, Newberry 1998, Gaspar and Inverno 2000).

Conclusions

The GS sheelite-bearing skarn developed at the contact of impure Lower Jurassic dolomitic and the Middle Jurassic Ghorveh granite during prograde and retrograde stages. The mineral assemblage and compositions of individual mineral species are affected by many factors including; magma-wall rock compositions, nature of derived magmatic hydrothermal fluids (especially F content), depth and temperature.

Elemental variation trend in the GS skarn clinopyroxene suggests that it has experienced local variations in Mg:Mn:Fe proportions due to changes in the pristine dolomitic host rock composition. The high johannsenite content in type Ib clinopyroxene indicates a local high Mn content in dolomitic host rock.

The high garnet/clinopyroxene abundance ratio implies the dominance of oxidizing condition, while presence of an F-rich volatile phase affects the zoning patterns and mineral abundances in the GS skarn. It is due to increase in Al solubility of the hydrothermal fluid and increase in vesuvianite abundance instead of clinopyroxene, resulting to high garnet/clinopyroxene ratios in the GS skarn. Also, the F-rich volatile phase acts as a catalyzer in scheelite deposition, which is not associated with the marble front or quartz veins, yet it is mostly related to the vesuvianite occurrence. Presence of a high grossular component in garnet, Mo-poor scheelite, hedenbergite- and diopside-rich clinopyroxene, pyrrhotite as the dominant sulfide mineral with later subcalcic garnets developement in the GS skarn, strongly resemble to moderately reduced scheelite-bearing skarns. Clinopyroxene and garnet co-occurrence and lack of replacement textures between them, indicate that prograde stage in the GS skarn formed at temperature range of 580 °C and 400 °C and $\log fO_2 = -18$ to -28.

Acknowledgments This work is part of the Ph.D thesis of Z.A. Authors would like to thank Marcello Serracino and Marco Albano for providing EPMA and SEM analyses (Sapienza University) and Tom Knott for XRF analyses (Leicester University). We are very grateful to Andy Saunders, Franz Neubauer, Hossein Azizi, and Mir-Saleh Mirmohammadi for their constructive comments on a preliminary draft of the manuscript. We acknowledge Franz Neubauer and Andy Saunders for English editing of the manuscript. Constructive comments by three anonymous reviewers, journal associate editors Paolo Stefano Garofalo and Christoph Hauzenberger and editor-in-chief Lutz Nasdala are gratefully acknowledged. Authors also would like to acknowledge partial financial support by the Ministry of Science, Research and Technology (MSRT), Kharazmi University and Iran National Science Foundation (Grant No. 91058052).

References

Abdi M (2007) Lithogeochemistry and genesis of mineralization at Deh-Hossein and Nezam-Abad W-Sn (Cu) deposits and comparison with Bamsar deposit, SW Shazand, Arak. MSc thesis, Tarbiat Modares University, Tehran (in Persian with English abstract)

Arai H (2010) A function for the R programming language to recast garnet analyses into end-members: Revision and porting of Muhling and Griffin's method. Comput Geosci-UK 36:406–409

Armbruster T, Bonazzi P, Akasaka M, Bermanec V, Chopin C, Giere R, Assbichiler SH, Liebscher A, Menchetti S, Pan Y, Pasero M (2006) Recommended nomenclature of epidote-group minerals. Eur J Mineral 18:551–567

Azizi H, Asahara Y (2013) Juvenile granite in the Sanandaj-Sirjan zone, NW Iran: Late Jurassic-Early Cretaceous arc-continent collision. Int Geol Rev 55:1523–1540

Azizi H, Chung SL, Tanaka T, Asahara Y (2011a) Isotopic dating of the Khoy metamorphic complex (KMC), northwestern Iran: a significant revision of the formation age and magma source. Precambrian Res 185:87–94

Azizi H, Asahara Y, Mehrabi B, Chung SL (2011b) Geochronological and geochemical constraints on the petrogenesis of high-K granite from the Suffiabad area, Sanandaj-Sirjan Zone, NW Iran. Chem Erde - Geochem 71:363–376

Azizi H, Beiranvand MZ, Asahara Y (2015a) Zircon U-Pb ages and petrogenesis of a tonalite-trondhjemite-granodiorite (TTG) complex in the Northern Sanandaj-Sirjan Zone, Northwest Iran: evidence for Late Jurassicarc-continent collision. Lithos 216-217:178–195

Azizi H, Najari M, Asahara Y, Catlos EJ, Shimizu M, Yamamoto K (2015b) U-Pb zircon ages and geochemistry of Kangareh and Taghiabad mafic bodies in northern Sanandaj-Sirjan Zone, Iran: Evidence for intra-oceanic arc and back-arc tectonic regime in Late Jurassic. Tectonophysics 660:47–64

Azizi H, Mohammadi K, Asahara Y, Tsuboi M, Daneshvar N, Mehrabi B (2016) Strongly peraluminous leucogranite (Ebrahim-Attar granite) as evidence for extensional tectonic regime in the Cretaceous, Sanandaj-Sirjan zone, northwest Iran. Chem Erde - Geochem 76: 529–541

Barati M (2012) Mineralogy, geochemistry and S isotope in Galali skarn deposit, W Iran. Iranian Journal of Crystallography and Mineralogy 20:215–228

Barati M, Gholipoor M (2014) Study of REE behaviors, fluid inclusions, and O, S stable Isotopes in Zafar-abad iron skarn deposit, NW Divandarreh, Kordestan province. J Econ Geol 6:5–6 (in Persian with English abstract)

Berger J, Femenias O, Mercier JCC, Demaiffe D (2005) Ocean floor hydrothermal metamorphism in Limousin ophiolites (Western French Massif Central): evidence of a rare preserved Variscan oceanic marker. J Metamorph Geol 23:795–812

Bozkurt E, Winchester JGA, Piper JDA (2000) Tectonics and Magmatism in Turkey and the Surrounding Area. Geol Soc London Spec Publ, no 173

Brown PE, Bowman JR, Kelly WC (1985) Petrologic and stable isotope constraints on the source and evolution of skarn-forming fluids at Pine Creek, California. Economic Geology 80(1):72–95

Burton JC, Taylor LA, Chou IM (1982) The fO_2-T and fS -T stability relations of hedenbergite and of hedenbergite-johannsenite solid solutions. Econ Geol 77:764–783

Capitani GC, Mellini M (2000) The johannsenite-hedenbergite complete solid solution clinopyroxenes from the Campiglia Marittima skarn. Eur J Mineral 12:1215–1227

Cepedal A, Martin-Izard A, Reguilón R, Rodriguez-Pevida L, Spiering E, Gonzălez-Nistal S (2000) Origin and evolution of the calcic and magnesian skarns hosting the El Valle-Boinăs copper-gold deposit, Asturias (Spain). J Geochem Explor 71(2):119–151

Chowdhury S, Lentz DR (2011) Mineralogical and geochemical characteristics of scheelite-bearing skarns and genetic relations between skarn mineralization and petrogenesis of the associated granitoid pluton at Sargipali, Sundergarh District, Eastern India. J Geochem Explor 108:39–61

Ciobanu CL, Cook NJ (2004) Skarn textures and a case study: the Ocna de Fier-Dognecea orefield, Banat, Romania. Ore Geol Rev 24(3): 315–370

Daneshvar N (2012) Lithogeochemistry of tungsten Ebrahim-Attar mineralization, southwest of Ghorveh, Iran. MSc thesis, Kharazmi University, Tehran (in Persian with English abstract)

Deer WA, Howie RA, Zussman J (1992) An introduction to the rock-forming minerals. 2nd edn. Longman, Burnt Mill, England, 696 pp

Dick LA, Hodgson CJ (1982) The MacTung W-Cu (Zn) contact metasomatic and related deposits of the northeastern Canadian Cordillera. Econ Geol 77:845–867

Dilek Y, Imamverdiyev N, Altunkaynak S (2010) Geochemistry and tectonics of Cenozoic volcanism in the Lesser Caucasus (Azerbaijan) and the peri-Arabian region: collision-induced mantle dynamics and its magmatic fingerprint. Int Geol Rev 52:536–578

Dimanov A, Wiedenbeck M (2006) (Fe, Mn)-Mg interdiffusion in natural diopside: effect of fO_2. Eur J Mineral 18:705–718

Dingwell DB, Brearley M (1985) Mineral chemistry of igneous melanite garnets from analcite-bearing volcanic rocks, Alberta, Canada. Contrib Mineral Petrol 90:29–35

Dobson DC (1982) Geology and alteration of the Lost River tin-tungsten-fluorine deposit, Alaska. Econ Geol 77:1033–1052

Einaudi MT, Burt DM (1982) Introduction-terminology, classification and composition of skarn deposits. Econ Geol 77:745–754

Einaudi MT, Meinert LD, Newberry RJ (1981) Skarn deposits. In: Skinner BJ (ed) Economic Geology Seventy-fifth Anniversary Volume. Soc Econ Geol, Boulder, pp 317–391

Falcon N (1974) Southern Iran: Zagros Mountains. In: Spencer, A.M., Ed., Mesozoic-Cenozoic Orogenic Belts. J Geol Soc Lond 4:199–211

Fonteilles M, Soler P, Demange M, Derre C, Krier-Schellen AD, Verkaeren J, Guy B, Zahm A (1989) The scheelite skarn deposit of Salau (Ariege, French Pyrenees). Econ Geol 84:1172–1209

Gamble RP (1982) An experimental study of sulfidation reactions involving andradite and hedenbergite. Econ Geol 77:784–797

Gaspar LM, Inverno CMC (2000) Mineralogy and metasomatic evolution of distal strata-bound scheelite skarns in the Riba de Alva Mine, Northeastern Portugal. Econ Geol 95:1259–1275

Ghorbani M (2007) Economic geology of mineral and natural resources of Iran. Arian Zamin, Tehran, p 492 (in Persian)

Ghorbani M (2013) The economic geology of Iran: mineral deposits and natural resources. Springer Science Business Media, Dordrecht, p 581

Gordon TM, Greenwood HJ (1971) The stability of grossular in H_2O-CO_2 mixtures. Am Mineral 56:1674–1688

Grammatikopoulos TA, Clark AH (2006) A comparative study of wollastonite skarn genesis in the Central Metasedimentary Belt, southeastern Ontario, Canada. Ore Geol Rev 29(2):146–161

Gray RF, Hoffman VJ, Bagan RJ, McKinley HL (1968) Bishop tungsten district, California. In: Ridge, J.D. (Ed.), Ore deposit of the United States, 1933–1967 (Graton-Sales vol.). New York, Am. Inst. Mining Metall. Petroleum Engineers, pp. 1531–1554

Greenwood HJ (1967) Wollastonite: Stability in H_2O-CO_2 mixtures and occurrence in a contact-metamorphic aureole near Salmo, British Columbia, Canada. Am Mineral 52:1669–1680

Gustafson WI (1974) The stability of andradite, hedenbergite, and related minerals in the system Ca-Fe-SiO-H. J Petrol 15(3):455–496

Hassanzadeh J, Stockli DF, Horton BK, Axen GJ, Stockli LD, Grove M, Schmitt AK, Walker JD (2008) U-Pb zircon geochronology of late Neoproterozoic. Early Cambrian granitoids in Iran: implications for paleogeography, magmatism, and exhumation history of Iranian basement. Tectonophysics 451:71–96

Hochella MF, Liou JG, Keskinen MJ, Kim HS (1982) Synthesis and stability relations of magnesium idocrase. Econ Geol 77:798–808

Hosseini M (1999) Geological map of Qorveh, scale 1:100000. Geological Survey of Iran

Jahns RH (1944) Ribbon rock, an unusual beryllium tactite. Econ Geol 39(3):173–205

Kamvong T, Zaw K (2009) The origin and evolution of skarn-forming fluids from the Phu Lon deposit, northern Loei Fold Belt, Thailand: evidence from fluid inclusion and sulfur isotope studies. J Asian Earth Sci 34(5):624–663

Kwak TAP (1986) Fluid inclusions in skarn (carbonate replacement deposits). J Metamorph Geol 4:363–384

Kwak TAP (1987) W-Sn skarns deposits and related metamorphic skarns and granitoids. Dev Econ Geol 24:451

Kwak TAP, Askins PW (1981) Geology and genesis of the F-Sn-W (-Be-Zn) skarn (wrigglite) at Moina, Tasmania. Econ Geol 76:439–467

Kwak TAP, Tan TH (1981) The geochemistry of zoning in skarn minerals at the king Island (Dolphin) mine. Econ Geol 76:468–497

Le Anderson PJ (1981) Calculation of temperature and X(CO_2) values for tremolite-Kfeldspar- diopside-epidote assemblages. Can Mineral 19:619–630

Leak BE (1978) Nomenclature of amphiboles. Mineral Mag 42:533–563

Lehrmann B, Oliver NH, Rubenach MJ, Georgees C (2009) The association between skarn mineralisation and granite bodies in the

Chillagoe region, North Queensland, Australia. J Geochem Explor 101(1):58
Liou JG (1974) Stability relations of andradite-quartz in the system Ca-Fe-Si-O-H. Am Mineral 59:1016–1025
Lummen GM, Verkaeren J (1986) Physicochemical study of skarn formation in pelitic rock, Costabonne peak area, eastern Pyrenees, France. Contrib Mineral Petrol 93:77–88
Mahmoudi S, Corfu F, Masoudi F, Mehrabi B, Mohajjel M (2011) U-Pb dating and emplacement history of granitoid plutons in the northern Sanandaj-Sirjan Zone, Iran. J Asian Earth Sci 41:238–249
Mathieson GA, Clark AH (1984) The Cantung E Zone scheelite skarn orebody, Tungsten, Northwest Territories; a revised genetic model. Economic Geology 79(5):883–901
Meinert LD (1987) Skarn zonation and fluid evolution in the Groundhog mine, Central mining district, New Mexico. Econ Geol 82:523–545
Meinert LD (1993) Igneous petrogenesis and skarn deposits. Geol Assoc Can Spec Pap 40:569–583
Meinert LD (1995) Compositional variation of igneous rocks associated with skarn deposits-chemical evidence for a genetic connection between petrogenesis and mineralization. Mineral Assoc Canada, Short Course Series 23:401–418
Meinert LD, Newberry RJ, Einaudi MT (1980) An overview of tungsten, copper, and zinc-bearing skarns in western North America U.S. Geological Survey Open-File Report 81-355:304–327
Meinert LD, Hedenquist JW, Satoh H, Matsuhisa Y (2003) Formation of anhydrous and hydrous skarn in Cu-Au ore deposits by magmatic fluids. Econ Geol 98:147–156
Meinert LD, Dipple GM, Nicolescu S (2005) World skarn deposits. Society of Economic Geologists, Econ Geol 100th Anniversary Volume 299–336
Mohajjel M, Fergusson C (2014) Jurassic to Cenozoic tectonics of the Zagros Orogen in northwestern Iran. Int Geol Rev 56(3):263–287
Mohajjel M, Fergusson C, Sahandi M (2003) Cretaceous-Tertiary convergence and continental collision, Sanandaj-Sirjan zone, western Iran. J Asian Earth Sci 21(4):397–412
Momenzadeh M (1976) Stratabound lead zinc ores in the lower Cretaceous and Jurassic sediments in the Malayer-Esfahan District (West Central Iran): litology, metal content, zonation and genesis PhD Thesis, University of Heidelberg, Heidelberg
Moon KJ (1983) The genesis of the Sangdong tungsten deposit, the Republic of Korea: Unpublished Ph.D. thesis, Hobart, University of Tasmania, 366 p
Nakano T (1989) Fluctuation model for compositional heterogeneity of skarn clinopyroxenes. Geochem J 23:91–99
Nakano T (1991) An antipathetic relation between the hedenbergite and johannsenite components in skarn clinopyroxene from the Kagata tungsten deposit, Central Japan. Can Mineral 29:427–434
Newberry RJ (1982) Tungsten-bearing skarns of the Sierra Nevada. I. The Pine Creek Mine. California Econ Geol 77:823–844
Newberry RJ (1983) The formation of subcalcic garnet in scheelite-bearing skarns. Can Mineral 21:529–544
Newberry RJ (1998) W- and Sn-skarn deposits. Mineral Assoc Canada, Short Course Series 26:289–335
Newberry RJ, Einaudi MT (1981) Tectonic and geochemical setting of tungsten skarn mineralization in Cordillera. In: Dickson WR, Payne, WD (eds) Relations of tectonics to ore deposits in the Southern Cordillera. XIV. AGS Digest:99–111
Newberry RJ, Swanson SE (1986) Scheelite skarn granitoids: an evaluation of the roles of magmatic source and process. Ore Geol Rev 1: 57–81
Newberry RJ, Allegro GL, Cutler SE, Hagen-Levelle JH, Adams DD, Nicholson LC, Weglarz TB, Bakke AA, Clautice KH, Coulter GA, Ford MJ, Myers GL, Szumigala DJ (1997) Skarn deposits of Alaska. Econ Geol Monogr 9:355–395
Newton RC (1966) Some calc-silicate equilibrium relations. Am J Sci 201:204–222
Orhan A (2017) Evolution of the Mo-rich scheelite skarn mineralization at Kozbudaklar, Western Anatolia, Turkey: Evidence from mineral chemistry and fluid inclusions. Ore Geol Rev 80:141–165
Paydar GR (2016) Polygenetic Iron Mineralization in the Baba-Ali and Galali Deposits, further evidences from stable (S, O, H) isotope data, NW Hamedan, Iran. International Journal of Geological and Environmental Engineering 10(2)
Paydar GR, Lotfi M, Ghaderi M, Amiri A, Vosooghi-Abedini M (2010) New results on mineralography and crystal chemistry of magnetite and pyrite at Baba-Ali & Galali iron deposits, west of Hamadan, Iran. GEOSCIENCES 20:121–130 (in Persian with English abstract)
Pouchou JL, Pichoir F (1984) A new model for quantitative analyses. I. Application to the analysis of homogeneous samples. La Rech Aérospatiale 3:13–38
Pouchou JL, Pichoir F (1985) "PAP" ($\varphi\rho$-Z) correction procedure for improved quantitative microanalysis. Microb Anal 203:104–106
Rasmussen KL, Lentz DR, Falck H, Pattison D RM (2011) Felsic magmatic phases and the role of late-stage aplitic dykes in the formation of the world-class Cantung Tungsten skarn deposit, Northwest Territories, Canada. Ore Geology Reviews 41(1):75-11110.2113/gsecongeo.80.1.72
Ravna EK (2000) The garnet-clinopyroxene Fe^{2+}-Mg geothermometer: an updated calibration. J Metamorph Geol 18:211–219
Robertson AHF, Parlak O, Rízaoğlu T, Ünlügenç Ű, İnan N, Tasli K, Ustaömer T (2007) Tectonic evolution of the South Tethyan Ocean: evidence from the Eastern Taurus Mountains (Elaziğ region, SE Turkey). J Geol Soc Lond 272:231–270
Salami S, Sepahi AA, Maanijou M (2013) Ebrahimattar pegmatite, skarn and related rocks. Iranian Journal of Crystallography and Mineralogy 2:309–322 (in Persian with English abstract)
Singoyi B, Zaw K (2001) A petrological and fluid inclusion study of magnetite–scheelite skarn mineralization at Kara, Northwestern Tasmania, Implications for ore genesis. Chem. Geol. 173, 239–253
Shahbazi H, Siebel W, Pourmoafee M, Ghorbani M, Sepahi AA, Shang CK, Abedini MV (2010) Geochemistry and U-Pb zircon geochronology of the Alvand plutonic complex in Sanandaj-Sirjan Zone (Iran): new evidence for Jurassic magmatism. J Asian Earth Sci 39:668–683
Shahbazi H, Siebel W, Ghorbani M, Pourmoafee M, Sepahi AA, Abedini MV, Shang CK (2015) The Almogholagh pluton, Sanandaj-Sirjan zone, Iran: geochemistry, U-(Th)-Pb titanite geochronology and implications for its tectonic evolution. Neues Jb Mineral Abh 192:85–99
Shakerardakani F, Neubauer F, Masoudi F, Mehrabi B, Liu X, Dong Y, Mohajjel M, Monfaredi B, Friedl G (2015) Pan-African basement and Mesozoic gabbro in the Zagros orogenic belt in the Dorud-Azna region (NW Iran): Laser-ablation ICP-MS zircon ages and geochemistry. Tectonophysics 647-648:146–171
Sheikhi F, Alaminia Z, Tabakh-Shabani AA (2012) Seranjic skarn geothermometery, SW Ghorveh, Kurdestan, Iran. Iranian Journal of Crystallography and Mineralogy 20:343–355 (in Persian with English abstract)
Shimazaki H (1977) Grossular- spessartine- almandine garnets from some Japanese scheelite skarns. Can Mineral 15:74–80
Shimazaki H (1980) Characteristics of skarn deposits and related acid magmatism in Japan. Econ Geol 75:173–183
Steven NM, Moore JM (1994) Pan-African tungsten skarn mineralization at the Otjua prospect, Central Namibia. Econ Geol 89:1431–1453
Stocklin J (1968) Structural history and tectonics of Iran: a review. AAPG Bull 52:1229–1258
Sweeney MJ (1980) Geochemistry of garnets from the North Ore shoot, Bingham district, Utah. MSc thesis, University of Utah, Salt Lake City

Timon Sanchez SM, Moro Benito MC, Cembranos Perez ML (2009) Mineralogical and physiochemical evolution of the Los Santos scheelite skarn, Salamanca, NW Spain. Econ Geol 104:961–995

Wesolowski D, Ohmoto H (1986) Calculated oxygen isotope fractionation factors between water and the minerals scheelite and powellite. Economic Geology 81(2):471–477

Wesolowski D, Cramer JJ, Ohmoto H (1988) Scheelite mineralization in skarns adjacent to Devonian granitoids at King Island, Tasmania, in Taylor RO, Strong DF, edn, Recent advances in the geology of granite related mineral deposits. Canadian Institute of Mining and Metallurgy 235-251

Whitney DL, Evans BW (2010) Abbreviations for names of rock-forming minerals. Am Mineral 95(1):185–187

Yajam S, Montero P, Scarrow JH, Ghalamghash J, Razavi SMH, Bea F (2015) The spatial and compositional evolution of the Late Jurassic Ghorveh-Dehgolan plutons of the Zagros Orogen, Iran: SHRIMP zircon U-Pb and Sr and Nd isotope evidence. Geol Acta 13:25–43

Yavuz F (2013) WinPyrox: A Windows program for pyroxene calculation classification and thermobarometry. Am Mineral 98:1338–1359

Zamanian H (2007) Geology of the Gelali iron mineralization related to the south Ghorveh batholith, western Iran. J Earth Sci 1:47–65

Zamanian H, Radmard K (2016) Geochemistry of rare earth elements in the Baba-Ali magnetite skarn deposit, western Iran-a key to determine conditions of mineralization. Geologos 22:33–47

Zaw K (1976) The CanTung E-zone orebody, Northwest Territories: A major scheelite skarn deposit. MSc thesis, Queen's University, Kingston

Zaw UK, Clark AH (1978) Fluoride-hydroxyl ratios of skarn silicates, Cantung E-zone scheelite orebody, Tungsten, Northwest Territories. Can Mineral 16:207–221

Zaw K, Singoyi B (2000) Formation of magnetite-scheelite skarn mineralization at Kara, Northwestern Tasmania: evidence from mineral chemistry and stable isotopes. Econ Geol 95:1215–1230

Zuo P, Liua X, Haob J, Wang Y, Zhao R, Ge S (2015) Chemical compositions of garnet and clinopyroxene and their genetic significances in Yemaquan skarn iron-copper-zinc deposit. Qimantagh, eastern Kunlun. J Geochem Explor 158:143–154